American Mineralogist, Volume 84, pages 1235–1255, 1999

Variability of apatite fission-track annealing kinetics: III. Extrapolation to geological time scales

RICHARD A. KETCHAM,[1,*] RAYMOND A. DONELICK,[2,†] AND WILLIAM D. CARLSON[1]

[1]Department of Geological Sciences, University of Texas at Austin, Austin, Texas 78712, U.S.A.
[2]Department of Geology and Geophysics, Rice University, Houston, Texas 77005, U.S.A.

ABSTRACT

A new model for examining fission-track data from natural specimens has been developed on the basis of new laboratory data describing fission-track annealing in a wide variety of apatites and the empirical correction for fission-track length anisotropy presented in earlier papers. Using revised and simplified statistical methods, we examine how well various empirical equations are able to fit the laboratory data and reproduce expected behavior on geological time scales. Based on the latter criterion, we find that so-called "fanning Arrhenius" models of mean track length are not the best-suited for our data. Instead, we find that fitting *c*-axis projected lengths with a model that incorporates some curvature on an Arrhenius plot produces results that are in better agreement with the available geological benchmarks. In examining the relative annealing behavior of apatites with different resistance to annealing, we find that the laboratory-time-scale behavior of any two apatites can be reproduced well by a simple one- or two-parameter equation. This function is used to convert the reduced fission-track length of one apatite that has undergone a certain time-temperature history into the length that would be measured in a second, less-resistant apatite that has undergone the same history. Using this conversion, we create a single model that encompasses the annealing behavior of all of the apatites we studied. The predictions made by this model match closely those made by fits to data for individual apatites. We therefore infer that, although the conversion equation is imperfect, it presents an excellent practical solution to characterizing the range of kinetic variability for annealing of fission tracks in apatite.

INTRODUCTION

One of the primary objectives in conducting apatite annealing experiments (e.g., Green et al. 1986; Crowley et al. 1991; Carlson et al. 1999, this volume) is to derive a model that describes the behavior of the apatite fission-track system over geological time scales (Laslett et al. 1987; Carlson 1990; Crowley et al. 1991; Laslett and Galbraith 1996). Such a model, when integrated with a computer program that allows fitting of data collected from natural specimens (Green et al. 1989b; Corrigan 1991; Willett 1992, 1997; Crowley 1993a; Gallagher 1995; Issler 1996), can be a very powerful tool for estimating past thermal histories. In favorable cases, detailed time-temperature paths can be derived using the track-length distribution to estimate the shape of the path while the central age constrains its placement in time.

However, an inherent weakness in earlier published annealing models is that they characterize only a single type of apatite. It has been well documented that different apatites can exhibit significantly different annealing behaviors. Green et al. (1989b) showed that apatites in the Otway Basin have differences in down-hole fading temperature of 30 °C or more. These changes in behavior are usually linked to compositional variations in apatite, with higher chlorine content leading to higher closure temperatures (Green et al. 1985, 1989b). However, we suggest that it is preferable to refer to this phenomenon as "kinetic" rather than "compositional" variation. There are three primary reasons for making this distinction. First, "kinetic" directly describes the observations: differences in annealing rates at laboratory and geological time scales. Composition can be used to infer kinetics, but the relationship is not straightforward, and currently there is no published physical model that can be used to link confidently specific compositional changes to kinetic effects. Second, annealing rates may be affected by factors in which composition plays a varying role. For example, increased chlorine content may enhance resistance to annealing in some cases by making intracrystalline diffusion require a higher activation energy, whereas increased contents of U and Th may inhibit annealing through continuous introduction of alpha recoil damage to the lattice. Third, changes in apatite behavior can be estimated without recourse to compositional data, by measuring apatite solubility using the diameter of the etch figures on the polished surface (Burtner et al. 1994; Donelick 1993, 1995). As shown below, this method provides roughly the same predictive capability as chlorine content, and is much less expensive and troublesome than microprobe analysis.

*E-mail: richk@maestro.geo.utexas.edu
†Current address: Department of Geology and Geological Engineering, University of Idaho, Moscow, Idaho 83844, U.S.A.

0003-004X/99/0009–1235$05.00

These kinetic variations commonly can be detected through the use of statistical tests (Green 1981), and in some cases kinetic subpopulations can be inferred and separated using statistically based graphical devices such as the radial plot. However, such methods only provide a measure of relative differences in behavior within a single group of apatites and do not allow comparison to other samples. Similarly, although they may be capable of roughly segregating apatites into broad kinetic classes, they provide no information about what the kinetic classes are. In the not uncommon case of a sample that contains apatites with a continuum of kinetic properties, statistical tests may indicate failure when in fact there are no inherent problems with the data. Finally, the statistical tests are applied only to fission-track ages, and there is no corresponding mechanism to separate fission-track length measurements unless every grain in which a track length is measured is also dated. These limitations apply to any approach that does not measure kinetic information for each apatite grain in which track density or track length is measured.

A monokinetic annealing model (one that assumes identical annealing behavior for all apatites) has serious shortcomings for studying natural samples with multikinetic apatite populations, as is the case in the majority of sedimentary rocks, and has been identified in some igneous rocks as well (O'Sullivan and Parrish 1995). First, use of monokinetic models implicitly assumes that the apatites being studied have the same kinetic behavior as the apatite that the model is based on, which is seldom the case, especially when a model based on the Durango apatite (e.g., Laslett et al. 1987) is employed. Second, pooling data from two or more kinetic subpopulations obscures the thermal history contained in each one. This problem is particularly severe in those parts of the time-temperature path in which some apatites have been totally reset while other, more resistant apatites still retain some older tracks. However, if the apatites can be separated correctly into kinetic populations that can each be modeled successfully and independently, the situation is transformed. The "single" apatite system then becomes a multiple one consisting of several independent thermochronometers, each with the ability to constrain the time at which the sample passed through a different temperature range. The objective of this paper is to take the initial steps toward developing a multikinetic model for apatite fission-track annealing that will make such interpretations possible and practical.

GEOLOGICAL BENCHMARKS

In evaluating and comparing apatite annealing models, it is not enough to judge among them based solely on how well they fit experimental data (e.g., Crowley 1993b). It is also important to take into account how well they match observations at the true scale of interest: over geological time. To gauge the usefulness of a model for studying data from unknowns, it must be evaluated against geological benchmarks. Although for most geochronometers, comparisons are made between experimentally derived and geologically inferred closure temperatures, complexities in the apatite fission-track system necessitate a closer look at the relevant concepts to summarize annealing model predictions accurately in a useful form. A useful geological benchmark consists of measured apatite data for which kinetic indicators have been collected as well, and that also has a past thermal history that can be reconstructed independently with some degree of confidence and precision. For apatite, there are two primary categories of interest: high-temperature and low-temperature. High-temperature benchmarks are useful for deriving information about the point at which fission tracks fully anneal, allowing assignment of the proper significance to fission-track ages. Low-temperature benchmarks are important for interpreting track-length data correctly, as they constrain the amount of annealing to be expected over long time scales in near-surface conditions.

Index temperatures in fission-track annealing

There is ambiguity in the fission-track literature about how to define and interpret the high-temperature annealing behavior of apatite. The traditional concept of closure temperature is only applicable to a subset of the cases in which fission-track data are used. Other circumstances that are somewhat unique to the apatite system, such as its low closure temperature and its utility in reconstructing detailed temperature histories without recourse to other systems, require other concepts to describe them. Here we try to clarify the issue by defining three index temperatures to describe annealing behavior, each of which is useful in a different situation. Each is defined in terms of an idealized thermal history (constant heating/cooling rate or isothermal).

Dodson (1973, 1979) defined the *closure temperature* (T_C) for an isotopic system as the temperature of the unknown at the time given by its apparent age. In theory, most geochronologic systems have a high-temperature state in which daughter products (atoms or fission tracks) cannot accumulate owing to diffusion (or annealing), a low-temperature state in which loss of daughter products is negligible, and a transitional state between the two that is marked by partial loss of daughter products. The closure temperature is somewhere within this transition zone, at a point in part linked to the cooling rate through this zone. The application of the concept of closure temperature to fission tracks in apatite is not straightforward, for three primary reasons. First, there are no geologically reasonable temperatures at which annealing is negligible (Donelick et al. 1990). Second, fission tracks anneal quickly at the relatively low temperatures found in the near-surface (<5 km depth) environment, where it is likely that many samples have experienced a complicated history that cannot be characterized by a single cooling rate. Third, apatite fission-track dates are regularly measured in samples collected from drill holes, where their present-day temperatures may be within the range of fast annealing. In this case, the closure temperature becomes not only a function of cooling (or heating) rate, but also the temperature of sample collection.

Another temperature that is useful in discussions of fission-track analysis is the *total annealing temperature* (T_A). As defined by Issler (1996), T_A is the temperature at which a fission-track population, which formed at an arbitrarily low temperature (–100 °C in Issler 1996), fully anneals for a given heating rate. Because the annealing equation is bi-directional in time, T_A is also the temperature at the time of the formation

of the oldest remaining track during an episode of linear cooling at the same rate from a high temperature above which apatite fission tracks are fully annealed to the specified arbitrary low temperature. For this study we take the arbitrary low temperature to be 20 °C, as opposed to the value used by Issler (1996), to give T_A the geological interpretation of being the highest temperature seen by the oldest remaining fission track in an outcrop sample that has undergone constant linear cooling. Thus, the T_A parameter serves to mark the highest temperature that fission-track data can constrain on a time-temperature path. To encompass the range of values potentially useful for interpreting geological data, we present T_C and T_A values assuming constant cooling rates of 100, 10, and 1 °C/Ma for each annealing model discussed.

A third temperature measure that has been used to characterize fission-track annealing is the *temperature of 100% fission-track fading* (T_F), the down-hole temperature at which fission-track density falls to zero (Naeser 1981; Gleadow and Duddy 1981). Traditionally, T_F has been interpreted as being the constant temperature necessary to anneal all fission tracks after a fixed amount of time, which is assigned using independent geological evidence, and values from different areas are compared using an Arrhenius diagram of the logarithm of heating time vs. inverse T_F (Naeser 1981; Gleadow and Duddy 1981; Harrison 1985). There is some ambiguity in this usage, however, because it neglects the fission tracks that have formed during the heating episode, which must have had a much shorter time to anneal. For example, according to the Durango apatite model of Laslett et al. (1987), pre-existing fission tracks will be annealed after 30 m.y. at 108 °C, but fission tracks formed during that period and retained are sufficient to provide an age of 5.3 Ma. A temperature of 118 °C would be required to reduce the modeled age to less than 1 Ma, but that temperature would have the same effect given an isothermal annealing interval of 3, 30, or 300 m.y. In the present study, we approximate T_F as the temperature required to anneal the reduced mean track length to a value of 0.41, the lowest value observed in any published annealing experiment to date in which more than 10 tracks were measured. For each annealing model, we report $T_{F,10}$, $T_{F,30}$, and $T_{F,100}$, the temperatures required to achieve this value after 10, 30, and 100 m.y. of isothermal heating.

High-temperature benchmark

Most geological studies that seek to constrain the annealing behavior of apatite consist of samples collected from drill holes (e.g., Naeser and Forbes 1976; Naeser 1981; Gleadow and Duddy 1981). At progressively greater depths and thus higher temperatures, fission tracks become more annealed, until at some temperature they are erased entirely. There are several keys to success in such studies, as follows.

First, down-hole temperatures must be accurate. Because of the thermal disturbance caused by drilling, commonly a correction must be applied to the measured temperatures. Unfortunately, the data and corrections seldom are reported in fission-track studies that seek to constrain fission-track annealing (e.g., Gleadow and Duddy 1981; Corrigan 1993).

Second, it must be possible to construct an independent time-temperature path for the samples in question. Doing so with certainty is an intractable problem in geology, and estimates generally involve many simplifying assumptions. The best-suited environments for this purpose are those in which it can be asserted confidently that at present the samples are at their maximum temperature since burial, as this minimizes the number of assumptions that must be made. Examples of such studies include the Otway Basin (Gleadow and Duddy 1981; Green et al. 1989a) and South Texas (Corrigan 1993). On the other hand, localities in which there has been significant cooling, such as Eielson Air Force Base (Naeser 1981), can be more problematic to interpret. The cooling path must be known in considerable detail, both to constrain the time when the apatites passed into the temperature range at which fission tracks are retained, and to determine the subsequent cooling rate.

Third, in view of the great influence that kinetic variability can have on fission-track annealing, it is crucial to measure kinetic indicators for all apatites studied. The only investigation for which this was done and for which some data are available in the literature is the Otway Basin study (Gleadow and Duddy 1981; Green et al. 1989a, 1989b). Although Corrigan (1993) determined the compositions of apatites in some of his samples, he did not take the necessary step of acquiring compositional data on each grain for which he measured an age or track length. In kinetically heterogeneous samples, an average apatite composition is not sufficient for a quantitative interpretation of annealing kinetics.

For the present analysis we use for a high-temperature benchmark published results from the Otway Basin (Gleadow and Duddy 1981; Green et al. 1985, 1989b; Green 1995). Basin analysis, along with complementary low-temperature data, has been used to infer that the deepest sample from the Flaxmans well has undergone the time-temperature history shown in Figure 1a (Gleadow and Duddy 1981). Green et al. (1989b) showed that end-member F-apatites in that well become fully annealed at a current down-hole temperature of 92 °C. Apatites found in Otway Basin wells have a compositional range from end-member F-apatite to apatites with at least 2.2 wt% Cl; these more Cl-rich apatites appear to retain tracks until temperatures of above 124 °C (Green 1995). Apatites with a chlorine content like Durango apatite (0.4 wt% Cl) show full annealing at approximately 95–100 °C (Green 1995). For the purposes of interpreting these results with respect to an annealing model, we use the approximation that the temperature at which a zero age is observed should correspond to the temperature $T_{F,30}$, as defined above.

It is also important to recognize, however, that not all published data are in agreement with the Otway Basin data. Although Corrigan (1993) did not obtain a full suite of compositional data, inspection of his single-grain age determinations shows that the lowest temperature at which any individual grains were totally annealed was 128 °C (Corrigan 1990). Stratigraphic reconstructions indicate that this sample (KY18), from the Frio growth fault trend, has been within 570 m of its current depth (or within about 14 °C of its current temperature, based on the present-day geothermal gradient) since approximately 14 Ma (Corrigan 1990). Even given the disparity in thermal histories between the Otway Basin and South Texas, calculations show that these two data sets are probably incompatible in their high-temperature

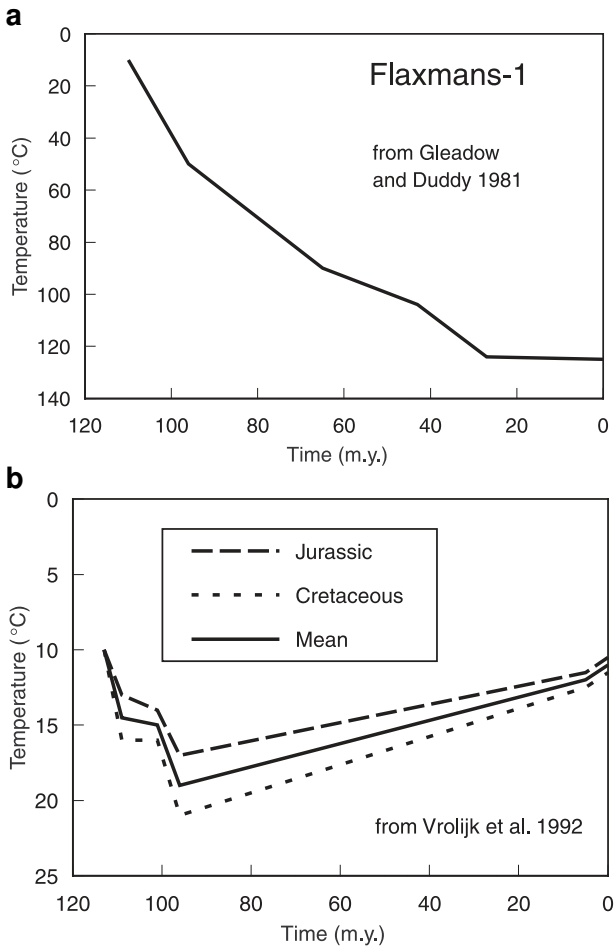

FIGURE 1. Time-temperature paths used to calculate comparisons of apatite fission-track annealing models to geological examples. (**a**) Flaxmans well, from the Otway Basin (Gleadow and Duddy 1981). (**b**) East Mariana Basin, from the Ocean Drilling Program Leg 129 (Vrolijk et al. 1992). Because the time of rifting in the area is not well constrained, two models are provided by Vrolijk et al. (1992). For this study, the average of the two paths is used.

predictions by about 15–20 °C. The source of this disparity is unknown; the most likely candidates are inaccurate down-hole temperature determinations and/or estimates of thermal history, although the lack of detailed compositional data for the South Texas samples admits the slight possibility that different kinetic classes may be involved.

Low-temperature benchmark

Although comparatively neglected in the literature to date, low-temperature benchmarks are also of central importance for confident modeling of time-temperature paths from fission-track data. At low levels of annealing, relatively wide swings in temperature cause relatively small changes in fission-track length. Because the temperature at which a sample was collected is often the only "known" part of the time-temperature path, interpretation based on an annealing model that inaccurately predicts near-surface annealing behavior will be forced to distort the recent time-temperature history to compensate. For example, the Laslett et al. (1987) Durango apatite model predicts mean track lengths in a sample that has undergone 20 million years of constant heating at 0, 10, and 20 °C to be 15.8, 15.6, and 15.4 μm, respectively, if one assumes an initial mean track length of 16.35 μm as measured by Green et al. (1986). Mean track length measurements of natural samples rarely give such high values; a characteristic "long" track length in a natural F-apatite sample is typically in the 14.0–14.6 μm range. According to the Laslett et al. (1987) model, a mean track length of 14.6 μm [as measured by Green (1988) for spontaneous tracks from the Durango apatite] would require 20 m.y. of heating at ~40 °C, and a length of 14.0 μm implies a temperature of ~52 °C for a 20 m.y. isothermal history. As a result, a time-temperature history calculated using the Laslett et al. (1987) model for an outcrop sample yielding a mean length of less than 15 μm would require a late cooling event to bridge the gap between the surface temperature and the considerably higher temperature required by the model for the observed amount of annealing. If the Laslett et al. (1987) model is in error, then such a cooling event, which might lead to an interpretation of a kilometer or more of unroofing, is a modeling artifact with no geological significance.

The best low-temperature benchmark to date is provided by Vrolijk et al. (1992), in which apatites obtained from drill cores of sea-floor sediments were studied. Because of the supposedly simple history undergone by sea-floor sediments compared to rocks from continental surfaces, past temperatures can be estimated with much greater confidence. Sediments from a drill core collected in the Ocean Drilling Program Leg 129 in the East Mariana Basin yielded near-end-member F-apatites (Cl = 0.13 wt%) with a mean track length of 14.6 ± 0.1 μm. Reconstruction of the burial history at that location suggests that the apatites experienced a fairly narrowly confined range of temperatures between 10 °C and 21 °C, as shown in Figure 1b (Vrolijk et al. 1992). Predictions made by F-apatite annealing models for the average time-temperature path in Figure 1b will be calculated for comparison to the measured value.

One significant difficulty in interpreting the Vrolijk et al. (1992) result is that the initial length of newly formed tracks in the apatite in that sample is unknown, as insufficient additional material was available for an induced length measurement. In the six near-end-member F-apatites described in Carlson et al. (1999, this volume), the observed initial mean induced track lengths range from 15.78 to 16.42 μm. This variation of more than 0.5 μm introduces an ambiguity of similar magnitude into estimates of the amount of annealing undergone by the Vrolijk et al. (1992) sample, and the amount of shortening predicted by an annealing model. To account for this when using the Vrolijk et al. (1992) benchmark value, we report model predictions as a range of values based on the reduced length calculated from the model multiplied by the maximum and minimum initial mean length values listed above.

Other low-temperature indicators include some apatite standards, such as Durango apatite with an age of 31.4 Ma (Naeser and Fleischer 1975) and a mean track length of 14.47 ± 0.06 μm [as measured by RAD using techniques described in Carlson et al. (1999, this volume)] and apatite from the Fish Canyon tuff, with an age of 27.8 Ma (Naeser et al. 1981) and a mean

track length of 15.35 ± 0.06 μm (as measured by RAD). Utilization of such results is impaired by the fact that these are not end-member F-apatites, with not only considerable Cl contents but other compositional variations with potentially significant kinetic effects as well (Carlson et al. 1999, this volume). Furthermore, there is uncertainty about the temperatures that these apatites experienced since deposition, making the modeling-based approach used to examine the Vrolijk et al. (1992) benchmark more problematic. On the other hand, these apatites have the advantage that the initial track length is known from experimental work. Because the observed mean track length of the Fish Canyon apatite is long compared to virtually all other natural examples, we assume here that it has had a low-temperature history of a constant 20 °C since deposition for comparison to models of the annealing behavior of Fish Canyon apatite that will be derived later in this paper.

Predictions of previous models

Table 1 shows calculations of the index temperatures and low-temperature benchmark lengths for several previously published annealing models. Figure 2 summarizes the predictions of some of these models as compared to our selected benchmarks. The widely used model of Laslett et al. (1987) of the Durango apatite data of Green et al. (1986) agrees well with the cited Otway Basin data for apatites of similar Cl content. However, the mean length range of 14.9 to 15.5 μm for the low-temperature history appears long, which may lead to spurious late cooling episodes when time-temperature histories are fit to data from unknowns, as discussed earlier. This result is accentuated when the initial track length of 16.21 μm for the Durango apatite measured in this study is used, for which the predicted length after the Vroijk et al. (1992) time-temperature history is 15.3 μm. The re-analysis of the Green et al. (1986) data set by Crowley et al. (1991) slightly improves the low-temperature benchmark, but appears to shift the high-temperature benchmark in the wrong direction. The two empirical models of the F-apatite studied by Crowley et al. (1991) match the low-temperature benchmark well, but predict $T_{F,30}$ values that are considerably above the 90–95 °C reported for the Otway Basin; interestingly, the Carlson (1993) model is in much closer agreement with this datum, although its prediction of the mean track length for the low-temperature history is probably too long. The improved statistical treatment of Laslett and Galbraith (1996) considerably lowers the index temperatures based on the F-apatite measurements of Crowley et al. (1991), but increases the predicted low-temperature-history length, although not to the point of being incompatible if the shortest initial track length is used.

A second observation is that extrapolations based on the F-apatite studied by Crowley et al. (1991) give higher temperatures than the Durango apatite data of Green et al. (1986), although they appear roughly equivalent when the improved statistical treatment of Laslett and Galbraith (1996) is compared to the Durango apatite modeling of Crowley et al. (1991). Such a result is not expected, as the Cl content of the Durango apatite suggests that it should be more resistant to annealing. Simultaneous annealing experiments of fluorapatite and Durango apatite described by Carlson et al. (1999, this volume) consistently indicate that the Durango apatite is more resistant to annealing on laboratory time scales, and annealing models fit to both of these data sets below also consistently predict that Durango apatite should still be somewhat more resistant to annealing over geological time. The Carlson et al. (1999, this volume) data for F-apatite seem in overall agreement with the Crowley et al. (1991) data, although there are apparent systematic differences between the new and old data sets for Durango apatite (Carlson et al. 1999, this volume). As discussed in Carlson et al. (1999, this volume), we believe that the Green et al. (1986) and Crowley et al. (1991) data sets are probably incompatible, and that the Crowley et al. (1991) data set is likely to be the more accurate.

Finally, the model of Carlson (1990, 1993) consistently predicts lower index temperatures and greater low-temperature lengths than the corresponding fanning Arrhenius empirical models. This is due to the fact that the Carlson (1990) model is very similar to a parallel Arrhenius model, and thus its predicted contours of constant annealing have considerably less spread when extrapolated to geological time scales. Analysis of the new data reported in Carlson et al. (1999, this volume) supports fanning of the annealing contours at laboratory time scales, and the geological benchmarks imply that this fanning probably persists to geological time scales as well. Fanning cannot be replicated in the physical model of Carlson (1990) without modification of the simplifying assumptions used to derive it; potential modifications that generate fanning are discussed below.

TABLE 1. Comparison of predictions of previous annealing models at geological time scales

Apatite	Data from	Fitted model	$T_{F,100}$	$T_{F,30}$	$T_{F,10}$	$T_{C,1}$	$T_{C,10}$	$T_{C,100}$	$T_{A,10}$	$T_{A,30}$	$T_{A,100}$	$l_{m,low\text{-}T}$*
Durango	Green et al. (1986)	Laslett et al. (1987)	96.8	103.9	110.6	97.6	112.4	128.4	113.6	128.2	144.0	14.89-15.49
		Crowley et al. (1991)	102.5	109.6	116.2	101.7	116.2	132.1	119.2	133.6	149.1	14.80-15.40
		Carlson (1990)	76.4	83.6	90.5	84.3	99.4	115.7	93.5	108.4	124.6	15.34-15.97
F-apatite B-5	Crowley et al. (1991)	Crowley et al. (1991)	120.7	127.1	133.0	116.1	129.0	143.1	136.3	149.3	163.1	14.40-14.98
		Laslett and Galbraith (1996)	101.8	108.5	114.9	102.1	115.8	130.7	118.0	131.8	146.6	14.62-15.21
		Carlson (1993)	81.3	88.7	95.6	84.7	99.4	115.4	98.6	113.8	130.3	14.99-15.60
Sr-F-apatite	Crowley et al. (1991)	Crowley et al. (1991)	136.5	142.8	148.7	126.9	139.8	153.6	152.0	164.7	178.3	14.26-14.84
		Laslett and Galbraith (1996)	133.1	139.5	145.5	123.4	136.4	150.5	148.7	161.7	175.5	14.30-14.88
		Carlson (1993)	94.1	101.5	108.7	96.3	111.3	127.5	111.6	127.1	143.8	15.13-15.74

* Assumed initial mean lengths for calculation of $l_{m,low\text{-}T}$ are based on measured results from Carlson et al. (1999, this volume) to best reflect that the low-temperature benchmark was measured by R.A. Donelick, and the range of possible initial mean length values for end-member F-apatite. In the six F-apatites described in Carlson et al. (1999, this volume), initial mean lengths range from 15.78 to 16.42 μm. For models by Laslett and Galbraith (1996), predictions are first converted to reduced lengths by dividing by 16.33 μm, and then multiplied by the above initial values.

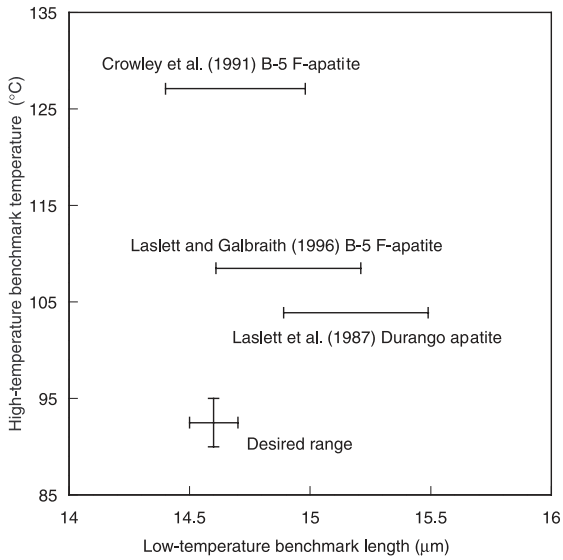

FIGURE 2. A comparison of predictions made by previous annealing models to the selected geological benchmarks described in the text, which are represented here by the "desired range." Models based on mean-length data for B-5 fluorapatite as measured by Crowley et al. (1991) may be able to reproduce the low-temperature benchmark, but appear to predict down-hole fading temperatures that are too high for the high-temperature one. The Durango apatite model of Laslett et al. (1987) may provide an acceptable fit to the high-temperature benchmark, once its Cl content is taken into account, but it predicts mean lengths that are significantly above the low-temperature benchmark. Time-temperature paths calculated using this relation for surface samples are thus more likely to require artificially high temperatures followed by a late cooling event to produce the amount of shortening often observed.

FITTING METHODS: INDIVIDUAL DATA SETS

There are fundamentally two approaches to modeling the annealing of fission tracks based on experimental results. The first is to utilize an empirical but kinetically reasonable equation to fit the data, as was done most successfully by Laslett et al. (1987), Crowley et al. (1991), and Laslett and Galbraith (1996) (see Laslett et al. 1987, for a review of earlier attempts). The second is to pose a theoretical physical model of fission-track annealing and use the experimental data to find values for the unknown parameters, each of which has a physical meaning (Carlson 1990). This latter approach has the advantage that, if correct, it allows for greater confidence in the extrapolation of experimental data collected in the laboratory over the course of days or months to geological time scales of millions of years. Furthermore, a physical model provides a much better basis for improving models of annealing, whether through gathering additional data, incorporation of fresh knowledge of atomic-scale processes, or simply the intuition that comes with being able to visualize a natural system. Offsetting these advantages is the possibility that the physical model is wrong in one or more respects, leading to spurious conclusions. It must also be recognized that the data being modeled are etched tracks, which are the product of at least three separate processes: track formation, track annealing, and chemical etching. In particular, vagaries in etching such as inter-laboratory differences in technique, etching anisotropy, and apatite composition may obscure details of the physical annealing process. As discussed above, the physical model of Carlson (1990) is not as successful in fitting the geological benchmarks as the empirical models, probably owing to the simplifications and assumptions used to derive it. As a result, we use only empirical functions in this paper, although physical implications are also considered.

The empirical annealing models can be reduced to the form:

$$g(l;l_0,\alpha,\beta) = f(t,T;C_i) \quad (1)$$

where g is a function that transforms lengths l using the initial track length l_0, which may be either a measured value (e.g., Laslett et al. 1987; Crowley et al. 1991) or a fitted parameter (Laslett and Galbraith 1996) and up to two fitted parameters α and β, and f is a function of time t and temperature T with a series of fitted parameters C_i. The semicolon is used here and below to separate input data on the left and fitted parameters on the right. Each half of this equation is dealt with separately.

Annealing models: Forms of $f(t, T; C_i)$

There have been two primary empirical models proposed for describing fission-track annealing: the parallel Arrhenius model and the fanning Arrhenius model (Laslett et al. 1987). Each defines a set of linear iso-annealing contours on an Arrhenius plot of log time vs. inverse temperature.

The parallel Arrhenius model consists of a set of parallel contour lines of constant reduced length. It has the form

$$f = C_0 + C_1 \ln(t) + C_2/T \quad (2)$$

where t is time in seconds, T is temperature in Kelvins, and C_0, C_1, and C_2 are fitted constants. The physical formulation of Carlson (1990) is nearly equivalent to a parallel Arrhenius model, with the difference that there is an additional factor of $\ln(T)$, leading to a slight curvature in the iso-annealing contours.

The fanning Arrhenius model has been the most successful at characterizing annealing data on laboratory time scales. The equation,

$$f = C_0 + C_1\left[\frac{\ln(t) - C_2}{(1/T) - C_3}\right] \quad (3)$$

defines a set of contours fanning from a single point. The fanning point in Arrhenius space ($\ln(t_0)$, $1/T_0$) is defined by C_2 and C_3. The original model posed by Laslett et al. (1987) was a form of this equation with the constant C_3, the $(1/T)$ coordinate of the fanning point, equal to zero. Crowley et al. (1991) found that their data could be characterized better if nonzero values for C_3 were allowed. In this paper, C_3 is allowed nonzero values although, in some cases, the best-fitting models converge to near-zero values for this parameter. The fractional term forms a roughly linear relation with the length transform g, and the purpose of the C_0 and C_1 terms is simply to fit that line. It is generally thought that the success of the fanning model indicates that the activation energy for track-length reduction somehow varies as a function of the track length, although this does not necessarily imply a direct causative relationship.

Crowley et al. (1991) proposed another model, which they termed a "fanning curvilinear" equation because it defines con-

tours of constant annealing that are slightly curved on a log time vs. inverse temperature plot:

$$f = C_0 + C_1\left[\frac{\ln(t) - C_2}{\ln(1/T) - C_3}\right]. \quad (4)$$

Crowley et al. (1991) discarded this form soon after proposing it, as it yields a slightly poorer fit when applied to their data. A similar result is observed in this study, but comparisons of model predictions to geological benchmarks indicate that this form deserves a closer look. Various physical implications of these models are considered in the discussion at the end of this paper.

The length transform: forms of $g(l; l_0, \alpha, \beta)$

In the simplest mathematical sense, for these empirical models, the purpose of transforming the length using an additional function g is to make it plot on a linear trend vs. the fractional term of the function f discussed above. In the first discussions of parallel Arrhenius models (Green et al. 1985; Laslett et al. 1987), it was noted that a plot of the function f vs. the reduced length r (= l/l_0) resembled a logarithmic curve, suggesting the transform:

$$g = \ln(1-r). \quad (5)$$

In introducing the fanning model, Laslett et al. (1987) also generalized the g function using a pair of power transformations of the form discussed by Box and Cox (1964):

$$g(r) = \left\{\left[\left(1 - r^{\beta}\right)/\beta\right]^{\alpha} - 1\right\}/\alpha \quad (6)$$

where α and β are fitted constants. This form was also used by Crowley et al. (1991), and we employ it here as well.

Laslett and Galbraith (1996) suggested a different form:

$$g(l) = \ln\left[1 - \left(l/l_0\right)^{1/\lambda}\right] \quad (7)$$

where l_0 (μ_{max} in Laslett and Galbraith 1996) is a parameter to be fitted, corresponding to the "true" initial track length before annealing within the reactor or at ambient room temperatures has taken place. Such an effect is suggested by the work of Donelick et al. (1990), which showed that up to 0.5 μm of annealing may take place at room temperature (23 °C) during the first month after irradiation. Laslett and Galbraith (1996) suggested that it is preferable that the same transformation be used for all apatites, and derived models based on the two data sets of Crowley et al. (1991) for F-apatite and Sr-F-apatite that have a common exponent $1/\lambda$ of 1/3.

The Laslett and Galbraith (1996) fitted values for l_0 are somewhat unexpected, however. For F-apatite, the fitted l_0 value was 16.71 μm, whereas the value measured by Crowley et al. (1991) was 16.34 μm, suggesting a 2.2% reduction in mean track length between the time of track formation and measurement. On the other hand, the Sr-F apatite had fitted and measured values of 18.96 and 16.33 μm, respectively, implying a reduction of 14.9%. Over the time interval from 3–10 minutes after a 37 second irradiation until 1–4 months later, Donelick et al. (1990) observed track-length reductions of 1.5–2.5% in two fluorapatites, Durango apatite, and Tioga apatite. Because of the interval between irradiation and etching, the total length reduction since initial track formation is larger to an unknown degree than was observed directly. The l_0 value fitted by Laslett and Galbraith (1996) for the initial lengths in F-apatite is similar to the measured values, but the fitted value for Sr-F-apatite is far above any observation or extrapolation of observed values. It should be recognized that the quantity estimated by Laslett and Galbraith (1996) is different from that measured by Donelick et al. (1990), and is also virtually unobservable. Furthermore, none of the apatites measured in Donelick et al. (1990) are Sr-apatites although, based on results reported here, the Tioga apatite is probably more resistant to annealing than the Crowley et al. (1991) Sr-apatite. While either of the l_0 values proposed by Laslett and Galbraith (1996) may arguably be reasonable if taken alone, they seem mutually inconsistent.

Implicit in the approach of Laslett and Galbraith (1996) is the assumption that a fanning linear empirical model reflects reality with sufficient precision that it can be used to extrapolate a prediction of initial length. If that model is insufficient or oversimplified (as may be argued based on results presented below), then their fitted parameters must vary to a certain extent to compensate for the errors that must inevitably result. It is reasonable to assume that such variations will corrupt the prediction of initial length, especially when it is considered that, when log-seconds are the unit of time, "instantaneous" time scales are as far removed from laboratory conditions as are geological ones. The fact that their predicted initial lengths appear to be inconsistent suggests that such corruption is a serious concern.

In this paper we exclusively use the g transform shown in Equation 6. Although simplifying the transform, as was done by Laslett and Galbraith (1996), is desirable when possible, the simplified forms we experimented with were incapable of producing good fits for the multi-apatite models presented later in this paper.

Merit functions

To arrive at the best set of fitted parameters, numerical procedures are used to minimize the misfit between f and g in Equation 1, using some merit function that has been selected to characterize the misfit. For their final models, both Laslett et al. (1987) and Crowley et al. (1991) maximize the log-likelihood function provided by Box and Cox (1964, Eq. 8). The Box and Cox (1964) formulation incorporates the assumption that after the transformation g has been applied to variable r, the error variance is constant. As discussed in Appendix A, which along with Appendix B is on deposit,[1] constant variance is not a valid assumption for fission-track annealing data. Laslett and Galbraith (1996) recognized this fact and derived an improved log-likelihood formulation that was customized for the description of fission-track data. However, their formulation is limited to certain functions f and g to which we did not wish to

[1]For a copy of Appendix A and B, document item AM-99-020, contact the Business Office of the Mineralogical Society of America (see inside front cover of recent issue) for price information. Deposit items may also be available on the American Mineralogist web site (http://www.minsocam.org or current web address).

be restricted. For this study we employ a χ^2 minimization scheme based on direct propagation of estimated errors. While not as sophisticated as the methods employed by Laslett and Galbraith (1996), it provides a simple and easily adaptable solution that closely reproduces their results, and can be extended to the additional models that we examine here. Details of the methods employed here are found in Appendix A.

Comparison of results from different fitting techniques

To investigate the differences that can arise from using the fitting techniques presented here as opposed to those in Laslett and Galbraith (1996), best-fit models were calculated for the data of Crowley et al. (1991), using a fanning Arrhenius model described by Equations 3 and 6. The resulting estimated parameters are shown in Table 2, as are the calculated index temperatures and track lengths for the models. In the case of the model for the B-5 fluorapatite, the fitting results provide geological time scale predictions that are nearly identical to those of the Laslett and Galbraith (1996) model shown in Table 1. All index temperatures are within 1.5 °C of each other, and the predictions for index lengths are within <0.1 μm of each other. The differences between the Sr-apatite models are somewhat larger, probably owing to the different forms of the $g(l)$ function. The high l_0 value predicted by Laslett and Galbraith (1996) alters the function in a way that precludes a close match by the functions used here. However, even in this case the maximum divergence in the index temperatures is <4 °C.

One other test was conducted to examine whether the inclusion of l_0 values from earlier in the annealing cycle could be a significant factor, using the only complete and self-consistent data set in which low-temperature annealing measurements were made by the same investigator on the same equipment, with the same etching conditions. The low-temperature annealing data for the Tioga apatite presented by Donelick et al. (1990) were combined with higher-temperature annealing experiments from Donelick (1991) and several additional unpublished data. Two fits were calculated, one using the "traditional" l_0 value corresponding to a measurement made at least a month after irradiation (16.77 μm), and another using the earliest value recorded, some 6 minutes after irradiation (17.08 μm). The resulting models are listed in Table 2. Although only the approach using the higher values for l_0 can reproduce measurements during the brief period of fission-track annealing in the days immediately following track formation, the difference between geologically relevant predictions is minor, as indicated by the <5 °C difference among the index temperatures.

Fitting results: Individual data sets

Previous studies have fit functions exclusively to the mean track length data from each experiment (e.g., l_m). The construction of a model to project track lengths to a common orientation parallel to the crystallographic *c* axis (Donelick et al. 1999, this volume), combined with the analysis of the Carlson et al. (1999, this volume) data to derive *c*-parallel lengths (l_c) properly, even on experiments that show segmentation (as was not done by Crowley et al. 1991), provides the additional capability of fitting functions to *c*-axis projected data. This latter approach has several significant conceptual advantages. First, in highly annealed samples there are probably at least two annealing processes at work, each of which has a profoundly different effect on track lengths: tip shortening and segmentation. Using *c*-axis projected lengths effectively removes the effects of segmentation, resulting in a model that only has to represent one annealing process, rather than a complex and variable combination of two as is contained in the mean length data. Second, mean lengths are affected by the relative frequency of track observations as a function of orientation. In most apatites it is very hard to see and thus measure tracks at low angles to the *c* axis, as they are very thin relative to tracks at higher angles; however, for some apatites with large etch figures (e.g., B2, B3, HS; Carlson et al. 1999, this volume) tracks at low angles are much easier to see, and are thus measured more frequently. Because within a single experi-

TABLE 2a. Fanning Arrhenius annealing models of previously published data sets obtained using χ^2 fitting, and their geological predictions: Index temperatures and lengths

Apatite	Data from	$T_{F,100}$	$T_{F,30}$	$T_{F,10}$	$T_{C,1}$	$T_{C,10}$	$T_{C,100}$	$T_{A,1}$	$T_{A,10}$	$T_{A,100}$	$l_{m,low-T}$
Durango	Green et al. (1986)	100.7	107.9	114.7	98.3	113.0	128.9	117.7	132.5	148.4	14.81–15.41
F-apatite B-5	Crowley et al. (1991)	102.6	109.4	115.8	102.0	115.8	130.7	118.9	132.9	147.8	14.68–15.28
Sr-F-apatite	Crowley et al. (1991)	129.5	135.9	141.9	121.5	134.6	148.7	145.1	158.2	172.0	14.26–14.84
Tioga	Donelick et al. (1991, unpub. data)	133.4	140.4	147.0	130.1	144.2	159.4	150.0	164.4	179.7	–
Tioga (including 23 °C experiments)	Donelick et al. (1990, 1991, unpub. data)	130.7	137.8	144.4	125.9	139.8	154.7	147.4	161.9	177.4	–

TABLE 2b. Fanning Arrhenius annealing models of previously published data sets obtained using χ^2 fitting, and their geological predictions: Model parameters

Apatite	Data from	χ^2_υ	C_0	C_1	C_2	C_3	α	β
Durango	Green et al. (1986)	4.05	–18.954 (02317)	0.00082385 (10992)	–28.143 (05233)	1.1217e-11 (2.4e-4)	–0.27951	–1.7910
F-apatite B-5	Crowley et al. (1991)	2.65	–22.971 (03389)	0.00097339 (14994)	–32.208 (07026)	3.1329e-11 (3.1e-4)	–0.43852	–6.4290
Sr-F-apatite	Crowley et al. (1991)	1.35	–9.9816 (09172)	0.00056272 (04133)	–6.1726 (16020)	1.1328e-03 (00590)	–0.12969	–33.394
Tioga	Donelick et al. (1991, unpub. data)	4.44	–16.964 (01329)	0.00063335 (04991)	–22.045 (02932)	4.5603e-04 (11016)	–0.60051	–4.4361
Tioga (including 23 °C experiments)	Donelick et al. (1990, 1991, unpub. data)	5.04	–21.454 (01936)	0.00078153 (07332)	–30.216 (04256)	1.4365e-04 (16214)	–0.81075	–1.8521

Note: Numbers in parentheses represent parameter variation within 95% confidence intervals.

ment tracks at low angles are always longer than tracks at high angles, this shift in observational frequency results in a shift in the mean track length. Projecting all tracks to a common orientation removes this bias entirely. A substantial corollary advantage is that l_c values within a single experiment are not as affected by Cf-irradiation (Donelick and Miller 1991) as mean lengths (Carlson et al. 1999, this volume).

However, there are also some disadvantages to modeling *c*-axis projected lengths. First, it is entirely possible that the equations that have been successful in describing annealing in terms of mean lengths are not the best suited for *c*-axis projected lengths. Furthermore, *c*-axis projected lengths show somewhat less organization on an Arrhenius plot relative to mean lengths, with more values being "out of place," making fitting an empirical equation more problematic. In most cases, this is caused by the relative scarcity of tracks at low angles, making the estimated *c*-axis intercept of the fitting ellipse more poorly determined when higher-angle tracks are lost to segmentation. Finally, it is not possible to measure l_c directly in most natural samples; at best, it can be estimated by measuring track length and angle using a conversion model such as that presented in Donelick et al. (1999, this volume). Our solution is to calculate a "modeled" *c*-axis projected track length ($l_{c,mod}$) by using the model to convert each individual track length in each experiment to its *c*-axis projected equivalent, and then taking the mean of these projected track lengths. This approach in effect processes the experimental data in exactly the same manner as that from natural specimens. The resulting values also are organized better on the Arrhenius plot. Results from fitting annealing models to the original l_c values tend to be quite similar to fits based on $l_{c,mod}$ when a reasonable fit is achieved.

Table 3 lists the results of fitting fanning linear and curvilinear empirical models to the principal data sets in Carlson et al. (1999, this volume). Because only non-Cf-irradiated measurements should be used for fitting mean-length data, the near-end-member hydroxyapatite HS was only fitted for $l_{c,mod}$. Owing to its very low uranium content and resulting sparsity of fission tracks, only 24 of its experiments did not undergo Cf-irradiation.

Several general trends are apparent in the fits. Comparison of the fanning linear fit of RN fluorapatite to the fit of the Crowley et al. (1991) B-5 F-apatite in Table 2 shows that they are very close in terms of their index temperatures, with all values within 4–5 °C of each other. This result corroborates the basic agreement between these two data sets. However, the RN fanning linear fit has a significantly longer estimate of the index length. Hydroxyapatite HS appears somewhat less resistant than fluorapatite. Durango apatite appears significantly more resistant to annealing than RN apatite on geological time scales, and the fit based on our Durango data predicts higher index temperatures than the one based on the data of Green et al. (1986) in Table 2. The end-member chlorapatite B3 is the most resistant of the four. The fits to $l_{c,mod}$ data predict 10–20 °C higher index

TABLE 3a. Annealing models of individual apatites from Carlson et al. 1999, this volume: Index temperatures and lengths

Apatite	Data fitted	Model type	$T_{F,100}$	$T_{F,30}$	$T_{F,10}$	$T_{C,1}$	$T_{C,10}$	$T_{C,100}$	$T_{A,1}$	$T_{A,10}$	$T_{A,100}$	T unc. (95%)	$l_{m,low-T}$
RN	l_m	F.A.	98.7	105.2	111.4	105.0	118.7	133.4	114.6	128.0	142.4	2.8-3.2	15.02–15.63
DR	l_m	F.A.	120.7	127.3	133.5	124.6	138.5	153.3	136.7	150.1	164.5	2.5-3.0	–
B3	l_m	F.A.	162.1	168.8	175.1	148.6	162.5	177.5	178.2	191.9	206.4	3.5-4.3	–
RN	l_m	F.C.	62.7	71.7	80.2	71.5	89.5	108.7	82.3	100.4	119.4	3.7-4.5	14.35–14.93
DR	l_m	F.C.	87.3	96.2	104.6	93.4	111.5	130.7	106.7	124.5	143.2	3.4-4.4	–
B3	l_m	F.C.	131.0	140.0	148.4	118.8	136.6	155.6	150.4	168.3	187.0	4.6-6.1	–
RN	$l_{c,mod}$	F.A.	115.6	122.3	128.7	123.6	137.9	153.2	131.8	145.5	160.2	2.6-3.6	15.06–15.67
DR	$l_{c,mod}$	F.A.	130.4	137.2	143.6	139.4	154.0	169.6	146.7	160.6	175.5	2.3-2.8	–
B3	$l_{c,mod}$	F.A.	166.8	173.5	179.9	165.9	180.2	195.4	183.0	196.6	211.2	2.8-3.3	–
HS	$l_{c,mod}$	F.A.	108.7	115.0	120.9	115.7	128.9	143.1	124.2	137.0	150.7	2.5-2.9	–
RN	$l_{c,mod}$	F.C.	82.6	91.6	100.1	91.9	110.5	130.3	102.1	120.2	139.2	3.4-4.9	14.37–14.95
DR	$l_{c,mod}$	F.C.	96.0	105.3	113.9	106.6	125.7	146.0	115.8	134.3	153.7	2.9-3.9	–
B3	$l_{c,mod}$	F.C.	134.2	143.1	151.5	135.0	153.3	172.6	153.5	171.3	189.9	3.5-4.4	–
HS	$l_{c,mod}$	F.C.	77.2	85.7	93.6	86.4	103.4	121.6	95.9	112.8	130.6	3.4-4.2	–

Notes: F.A. = Fanning Arrhenius model. F.C. = Fanning curvilinear model. T unc. (95%) = 95% bounds of uncertainty in index temperatures based on Monte Carlo simulations.

TABLE 3b. Annealing models of individual apatites from Carlson et al. 1999, this volume: Model parameters

Apatite	Data	Model	χ^2_u	C_0	C_1	C_2	C_3	α	β
RN	l_m	F.A.	3.18	–31.517 (04809)	0.0012879 (01953)	–34.001 (07263)	0.0000 (0.0002967)	–0.49032	–7.8453
DR	l_m	F.A.	3.23	–23.308 (03808)	0.00088138 (14166)	–24.752 (06643)	0.00044680 (23714)	–0.41011	–8.2670
B3	l_m	F.A.	1.16	–10.789 (01082)	0.00046806 (04347)	–9.3701 (23161)	0.00098792 (08967)	–0.16846	–18.246
RN	l_m	F.C.	3.31	–1394.1 (13562)	30.717 (29283)	–3286.6 (00132)	–79.069 (05875)	–0.41718	1.7251
DR	l_m	F.C.	3.23	–106.18 (06145)	2.1965 (12263)	–155.90 (01311)	–9.7864 (05925)	–0.48078	–6.3626
B3	l_m	F.C.	1.27	–18.926 (03303)	0.42290 (07361)	–27.239 (13509)	–7.1547 (56283)	–0.21650	–14.923
RN	$l_{c,mod}$	F.A.	4.82	–20.870 (03191)	0.00077447 (13506)	–26.133 (06801)	0.00033359 (27898)	–0.31430	–3.1361
DR	$l_{c,mod}$	F.A.	3.99	–24.640 (03567)	0.00091263 (13335)	–26.282 (05933)	0.00036602 (21873)	–0.36289	–9.1840
B3	$l_{c,mod}$	F.A.	1.46	–11.100 (00798)	0.00045168 (02862)	–9.6524 (16329)	0.00098362 (05497)	–0.17083	–21.024
HS	$l_{c,mod}$	F.A.	5.41	–15.061 (01661)	0.00061584 (06814)	–13.255 (03104)	0.00089793 (11956)	–0.36938	–15.272
RN	$l_{c,mod}$	F.C.	5.11	–61.311 (24309)	1.2920 (05296)	–100.53 (01330)	–8.7225 (57857)	–0.35878	–2.9633
DR	$l_{c,mod}$	F.C.	4.05	–105.48 (04950)	2.2022 (10386)	–153.47 (01300)	–9.7928 (59499)	–0.41712	–7.8961
B3	$l_{c,mod}$	F.C.	1.57	–19.418 (02284)	0.42147 (04704)	–26.870 (13355)	–7.1406 (56160)	–0.21704	–18.736
HS	$l_{c,mod}$	F.C.	5.48	–32.672 (07333)	0.68761 (15185)	–40.965 (13606)	–7.3822 (56096)	–0.45446	–11.843

Notes: F.A. = Fanning Arrhenius model. F.C. = Fanning curvilinear model. Numbers in parentheses represent parameter variation within 95% confidence intervals.

temperatures and longer index lengths compared to fits using mean lengths.

As also reported by Crowley et al. (1991), in almost all cases the fanning curvilinear models fit the experimental data slightly less well than the fanning Arrhenius models. In general, the fanning curvilinear models predict lower index temperatures and shorter low-temperature lengths as compared to the corresponding fanning Arrhenius models. This is an expected result of the relative forms of the iso-annealing contours predicted by each model; the fanning curvilinear model contours have a consistent curvature on an Arrhenius plot that causes them to predict lower resistance to annealing on all geological time scales. It should be noted that the $l_{c,mod}$ models are based on a larger number of experiments because they include measurements from Cf-irradiated mounts.

Of the four RN fluorapatite models listed in Table 3, the one that is closest to the high-temperature benchmark is the fanning curvilinear fit to the $l_{c,mod}$ data. The low-temperature benchmark length is also well within the bounds of the modeled range, unlike the linear fanning Arrhenius models. This is illustrated in Figures 3c and 3d, which show that a certain amount of curvature of the contours of constant annealing appears to be necessary to reconcile the laboratory measurements with field observations. Thus, even though the fanning curvilinear model does not statistically describe the experimental data as closely as a fanning Arrhenius model, we judge that it is the more justifiable one for deriving time-temperature paths for fluorapatites on geological time scales, at least based on the very limited evidence available in the literature at this time.

TOWARD A MULTIKINETIC MODEL: APATITE-APATITE COMPARISON

An important insight into the relative annealing properties of different apatites can be obtained by studying the results of experiments in which more than one apatite is annealed simultaneously, ensuring that they have had identical thermal histo-

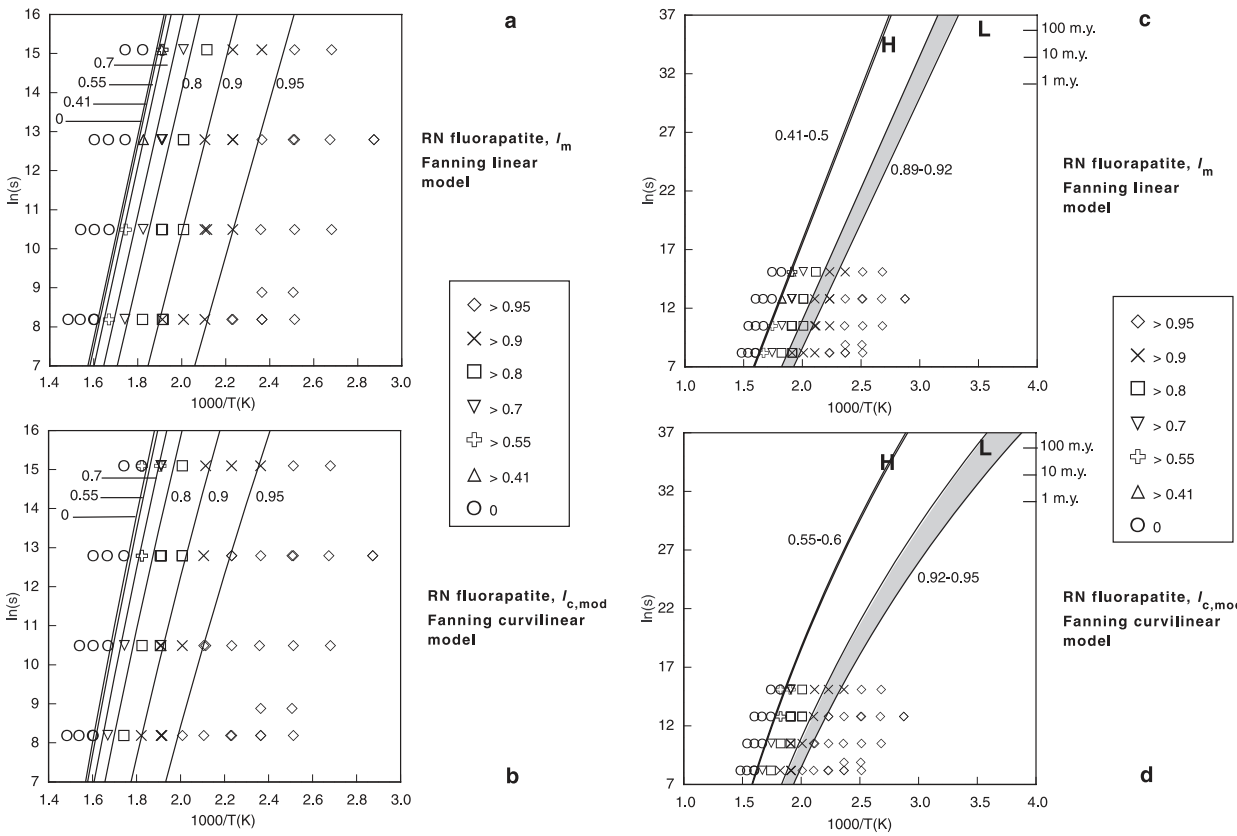

FIGURE 3. Fits of empirical models to end-member fluorapatite RN. (**a**) Fanning linear fit to the mean length data, the form of the model primarily used in previous studies of fission-track annealing. (**b**) Fanning curvilinear fit to the modeled *c*-axis projected data. The curvature in the contour lines is not apparent on laboratory time scales. (**c**) and (**d**) Extrapolations of these two models to geological time scales, along with how well they intersect the approximate positions of the selected geological benchmarks. "H" marks the area of time-temperature space that should coincide with fission-track fading as implied by the down-hole fading temperature data from the Otway Basin. "L" marks the approximate time-temperature area implied by the low-temperature annealing results of Vrolijk et al. (1992) from sea-floor sediments. The contours extended from laboratory to geological time scales correspond to roughly equivalent amounts of annealing for the two different types of track length data. The fanning linear model (**c**) consistently predicts a higher resistance to annealing than is indicated from the geological benchmarks, whereas the curvilinear model (**d**) intersects them both.

ries, and probably etching conditions as well (insofar as they were likely to have been etched at the same time). Figure 4 shows the relationship between the two apatites studied by Crowley et al. (1991), as well as similar plots for the four largest data sets reported by Carlson et al. (1999, this volume). With perhaps a single exception, the Crowley et al. (1991) data cluster around a consistent trend, and the data from the present study are also very well-behaved. The one outlier in the Crowley et al. (1991) data set, with experimental conditions of 340 °C and 1 hour, was also noted by Laslett and Galbraith (1996); it is likely that there may be a problem with this experiment for the B-5 fluorapatite, which has a mean length that is longer than expected when compared with results for other experiments at the same time and nearby temperature conditions.

A simple function can be used to characterize the relationship of one apatite to another at laboratory time scales:

$$r_{lr} = \left(\frac{r_{mr} - r_{mr0}}{1 - r_{mr0}} \right)^{\kappa} \quad (8)$$

where r_{lr} and r_{mr} are the reduced lengths of the apatites that are less resistant and more resistant to annealing, respectively, and r_{mr0} and κ are fitted parameters. In particular, r_{mr0} is the reduced length of the more resistant apatite at the point where the less resistant apatite first becomes totally annealed. This relationship appears to be able to characterize any pair of apatites, both with respect to mean length and *c*-axis projected length data.

A further insight into the possible meaning and utility of the r_{mr0} and κ parameters can be gained by inspecting the results obtained when the full range of apatites in this study are fitted individually to the B2 apatite, which is the most resistant (Table 4 and Fig. 5). The closeness of the best-determined val-

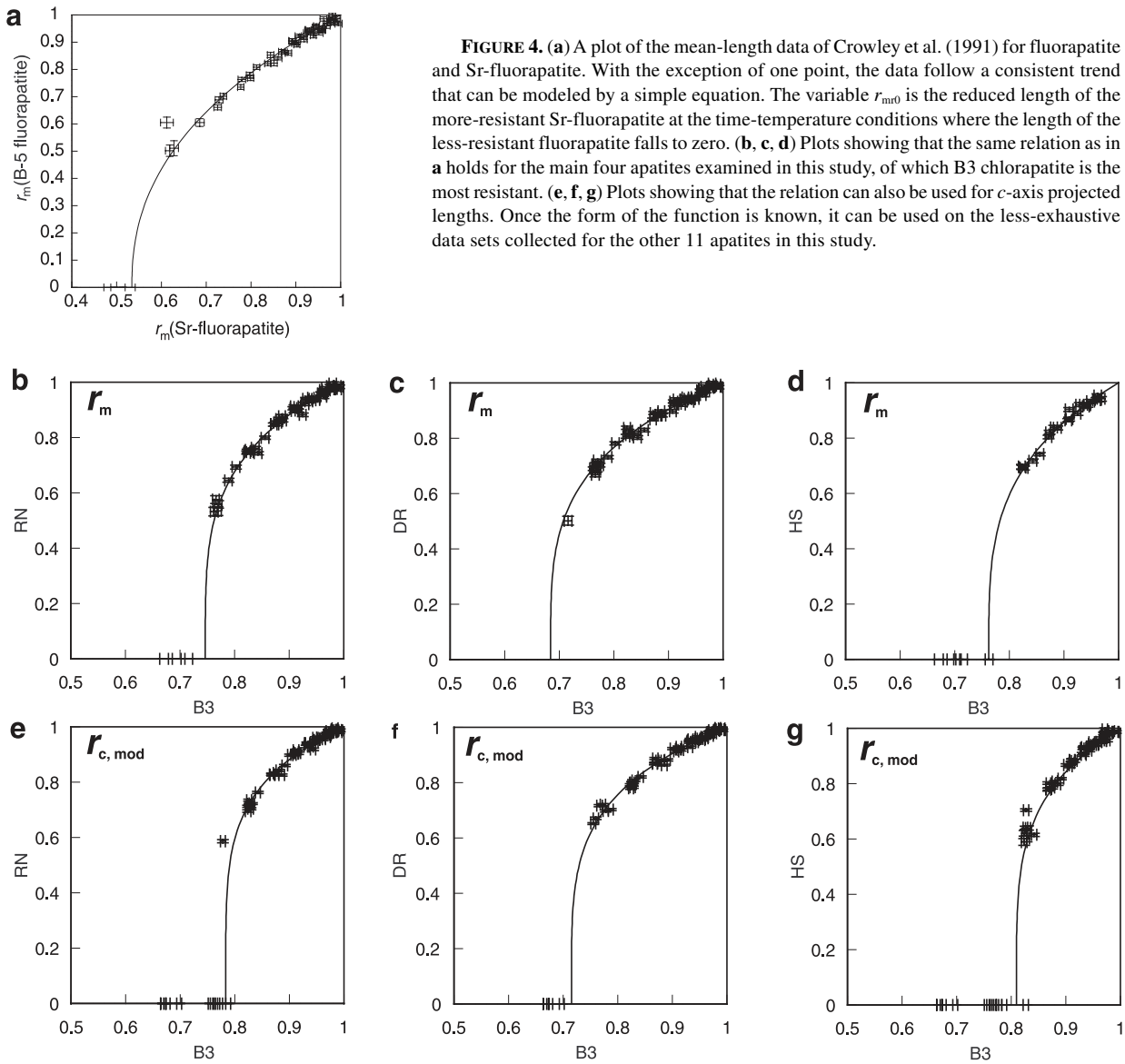

FIGURE 4. (**a**) A plot of the mean-length data of Crowley et al. (1991) for fluorapatite and Sr-fluorapatite. With the exception of one point, the data follow a consistent trend that can be modeled by a simple equation. The variable r_{mr0} is the reduced length of the more-resistant Sr-fluorapatite at the time-temperature conditions where the length of the less-resistant fluorapatite falls to zero. (**b**, **c**, **d**) Plots showing that the same relation as in **a** holds for the main four apatites examined in this study, of which B3 chlorapatite is the most resistant. (**e**, **f**, **g**) Plots showing that the relation can also be used for *c*-axis projected lengths. Once the form of the function is known, it can be used on the less-exhaustive data sets collected for the other 11 apatites in this study.

TABLE 4a. Fitted parameters for Equation 8 on paired mean length (l_m) data

		Individually fit							
ap1	ap2	num	χ^2_υ	r_{mr0}	± (95%)	κ	± (95%)	num	χ^2_υ
B2	AY	11	2.00	0.7557	+0.0160 / –0.0160	0.2599	+0.0429 / –0.0429	1248	2.57
B2	B3	11	0.72	0.5576	+0.1420 / –0.1778	0.5070	+0.2820 / –0.2180	1248	2.57
B2	DR	11	1.52	0.7613	+0.0115 / –0.0115	0.2361	+0.0346 / –0.0346	1248	2.57
B2	FC	11	0.42	0.6763	+0.0588 / –0.0619	0.3277	+0.1003 / –0.0934	1248	2.57
B2	HS	0	–	–	–	–	–	1248	2.57
B2	KP	11	2.78	0.6518	+0.1011 / –0.1377	0.3288	+0.1908 / –0.1509	1248	2.57
B2	OL	11	1.47	0.7739	+0.0104 / –0.0104	0.2972	+0.0365 / –0.0365	1248	2.57
B2	PC	11	2.49	0.4341	+0.2191 / –0.3681	0.5548	+0.4452 / –0.2744	1248	2.57
B2	PQ	11	2.44	0.7674	+0.0113 / –0.0113	0.2961	+0.0360 / –0.0360	1248	2.57
B2	RN	11	0.24	0.8303	+0.0133 / –0.0133	0.1686	+0.0326 / –0.0326	1248	2.57
B2	SC	11	0.75	0.8287	+0.0170 / –0.0170	0.1659	+0.0372 / –0.0372	1248	2.57
B2	TI	11	0.63	0.2971	+0.2335 / –0.1904	0.8085	+0.1915 / –0.3229	1248	2.57
B2	UN	11	1.12	0.8110	+0.0270 / –0.0270	0.2188	+0.0606 / –0.0606	1248	2.57
B2	WK	11	1.99	0.8186	+0.0211 / –0.0211	0.1870	+0.0460 / –0.0460	1248	2.57

TABLE 4b. Fits parameters for Equation 8 on paired modeled *c*-axis projected length ($l_{c,mod}$) data

		Individually fit							
ap1	ap2	num	χ^2_υ	r_{mr0}	± (95%)	κ	± (95%)	num	χ^2_υ
B2	AY	11	3.54	0.8198	+0.0158 / –0.0158	0.1766	+0.0336 / –0.0336	1436	2.82
B2	B3	11	0.86	0.6977	+0.0890 / –0.1270	0.3504	+0.1971 / –0.1465	1436	2.82
B2	DR	11	2.44	0.8204	+0.0142 / –0.0142	0.1675	+0.0303 / –0.0303	1436	2.82
B2	FC	11	0.41	0.7365	+0.0673 / –0.0673	0.2594	+0.0971 / –0.0928	1436	2.82
B2	HS	11	1.13	0.8822	+0.0086 / –0.0086	0.1267	+0.0247 / –0.0247	1436	2.82
B2	KP	11	3.77	0.7305	+0.0745 / –0.0833	0.2479	+0.1150 / –0.1068	1436	2.82
B2	OL	11	2.42	0.8386	+0.0115 / –0.0115	0.1873	+0.0312 / –0.0312	1436	2.82
B2	PC	11	1.68	0.3534	+0.3534 / –0.3534	0.6348	+0.3652 / –0.3652	1436	2.82
B2	PQ	11	3.17	0.8320	+0.0079 / –0.0079	0.1919	+0.0217 / –0.0217	1436	2.82
B2	RN	11	0.37	0.8787	+0.0103 / –0.0103	0.1064	+0.0212 / –0.0212	1436	2.82
B2	SC	11	3.16	0.8425	+0.0111 / –0.0111	0.1748	+0.0315 / –0.0315	1436	2.82
B2	TI	11	0.85	0.2632	+0.3378 / –0.1978	0.8142	+0.1858 / –0.4161	1436	2.82
B2	UN	11	2.56	0.8332	+0.0097 / –0.0097	0.1991	+0.0266 / –0.0266	1436	2.82
B2	WK	11	3.97	0.8358	+0.0118 / –0.0118	0.1834	+0.0301 / –0.0301	1436	2.82

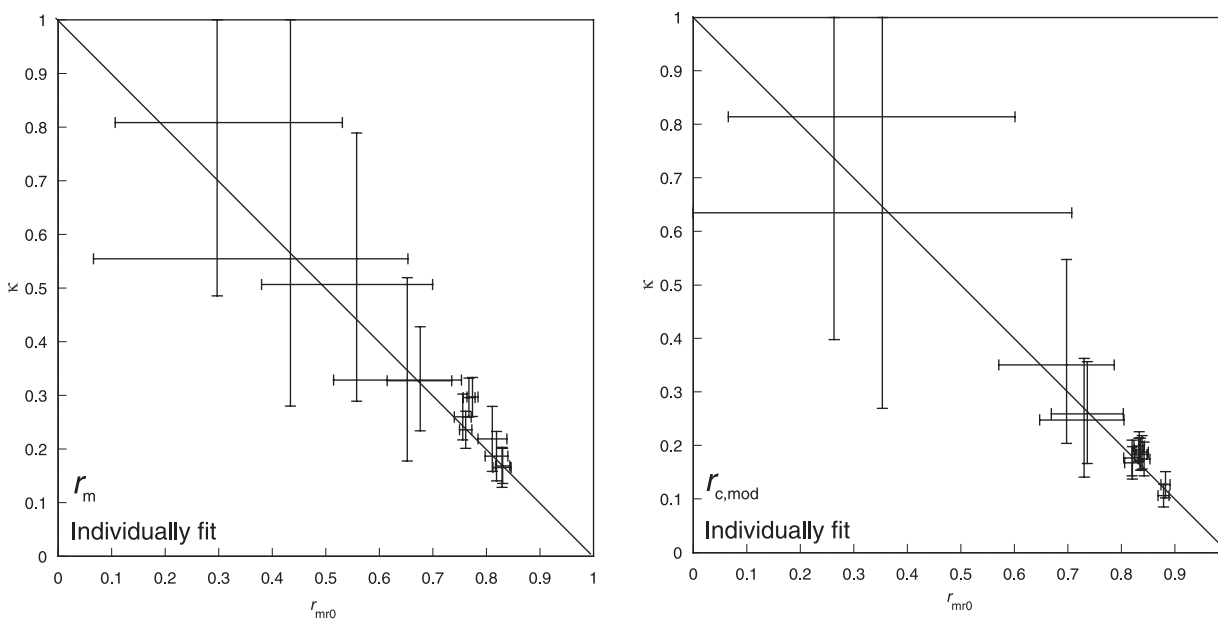

FIGURE 5. Relation between the paired experiment fitting parameters r_{mr0} and κ for all of the apatites in this study. The values fit to individual pairs are used here (Table 4, left column), although the values fit to all apatites simultaneously also show a similar trend. The closeness of the values to the diagonal line suggests the idealization $r_{mr0} + \kappa = 1$.

TABLE 4a.—*Extended*

Simultaneously fit			
r_{mr0}	± (95%)	κ	± (95%)
0.7507	+0.0134 / –0.0134	0.2803	+0.0299 / –0.0299
0.4436	+0.1332 / –0.1919	0.6855	+0.2476 / –0.2027
0.7625	+0.0094 / –0.0091	0.2491	+0.0190 / –0.0190
0.6227	+0.0842 / –0.0921	0.4072	+0.1478 / –0.1362
0.8067	+0.0074 / –0.0074	0.2872	+0.0181 / –0.0181
0.5718	+0.1287 / –0.1632	0.4399	+0.2198 / –0.1845
0.7771	+0.0097 / –0.0097	0.3040	+0.0260 / –0.0260
0.0522	+0.3837 / –0.0523	1.0000	+0.0000 / –0.4628
0.7635	+0.0106 / –0.0082	0.3276	+0.0324 / –0.0324
0.8000	+0.0068 / –0.0068	0.2537	+0.0166 / –0.0166
0.8046	+0.0103 / –0.0103	0.2331	+0.0252 / –0.0252
0.1447	+0.0916 / –0.0564	1.0000	+0.0000 / –0.1259
0.7736	+0.0117 / –0.0071	0.3083	+0.0308 / –0.0328
0.7815	+0.0132 / –0.0132	0.2753	+0.0373 / –0.0373

TABLE 4b.—*Extended*

Simultaneously fit			
r_{mr0}	± (95%)	κ	± (95%)
0.8237	+0.0101 / –0.0101	0.1753	+0.0208 / –0.0208
0.7106	+0.0514 / –0.0514	0.3329	+0.0768 / –0.0768
0.8271	+0.0081 / –0.0075	0.1636	+0.0166 / –0.0166
0.7547	+0.0425 / –0.0425	0.2369	+0.0627 / –0.0627
0.8559	+0.0041 / –0.0041	0.2206	+0.0088 / –0.0131
0.7492	+0.0493 / –0.0493	0.2265	+0.0646 / –0.0646
0.8364	+0.0063 / –0.0054	0.1958	+0.0183 / –0.0183
0.1678	+0.4361 / –0.1678	0.8331	+0.1669 / –0.5158
0.8273	+0.0065 / –0.0065	0.1991	+0.0134 / –0.0134
0.8464	+0.0052 / –0.0052	0.1787	+0.0105 / –0.0134
0.8401	+0.0064 / –0.0064	0.1840	+0.0157 / –0.0163
0.1398	+0.4606 / –0.0254	0.9665	+0.0335 / –0.5982
0.8343	+0.0067 / –0.0067	0.1952	+0.0188 / –0.0188
0.8369	+0.0058 / –0.0058	0.1806	+0.0161 / –0.0161

ues to the indicated line suggests the simplification

$$r_{mr0} + \kappa \cong 1 \tag{9}$$

which offers the interesting possibility that the behavior of any two apatites can be related by a single parameter. If this equality holds true, then Equation 8 can be simplified and reorganized to read:

$$1 - r_{mr} = \frac{1 - r_{lr}^{\beta}}{\beta} \tag{10}$$

where $\beta = 1/\kappa$, which is identical to a single Box-Cox transform. Attempts to impose this simplification across all apatites simultaneously result in significantly worse fits to the data, unfortunately, and we thus kept the variables independent for the models reported here. However, insofar as Equation 10 apparently expresses an overall trend in the data, we reserve its use for our final models that describe apatites in general rather than any specific variety.

Values for r_{mr0} and κ can either be fit for a single pair of apatites, or a set of r_{mr0}-κ pairs can be fitted for an entire suite of apatites simultaneously based on a single most-resistant apatite, improving the internal consistency of the set of values. Rather than only comparing each less-resistant apatite to the most-resistant apatite, a simultaneous solution takes into account how well each pair of less-resistant apatites matches up against each other when mapped to the most-resistant apatite. This approach also allows all of the paired experiments to be used, and not only those in which the most-resistant apatite was annealed simultaneously. Fitting procedures are discussed in greater detail in Appendix B. Results are shown on the right-hand side of Table 4; the difference from the individually fit values is caused primarily by the influence of the much larger numbers of experiments for apatites B3, RN, DR, and HS, although the constraints imposed by the simultaneous solution of the other apatites exert some influence as well.

There are several potentially large advantages in using Equation 8 to characterize the annealing of kinetically different apatites. First, it makes it possible to fit a single annealing model to all types of apatite. A single equation can be used to describe the most-resistant apatite, and then measured r_{mr0}-κ pairs can be used to infer the behavior of any less-resistant apatite. This unified-model approach also provides an easy means to interpolate between the behavior of apatites that have been measured in the laboratory; rather than having to measure all possible compositions of apatite, it is instead possible to create functions that relate r_{mr0} and κ to measurable kinetic parameters. Another advantage to this approach is that it makes it unnecessary to conduct 50 or more experiments on an apatite to have a database sufficient to produce a well-constrained empirical model. Instead, 10–15 well-chosen experiments paired with an apatite that has already been studied and incorporated into a unified model are all that is required to estimate values for r_{mr0} and κ.

It should be noted that there are at least two demonstrable inexactitudes to Equation 8 when it is used to characterize a suite of apatites. First, although it appears to work on any pair of apatites, there is no exact conversion between results if two different "most-resistant" apatites are used. For example, in a set of three apatites, designated A, B, and C in order of decreasing resistance to annealing, the result of converting lengths of apatite A to lengths of apatite C by fitting A to B and then B to C must be slightly different than the result of fitting A directly to C; it is mathematically impossible for these two paths to arrive at identical answers. Fortunately these differences seem minor, even when propagated to geological time scales. Second, because the equation is posed as a function of the reduced track length r, there is a strong dependence on initial track length, when in fact there is some doubt about how the initial track length should be best defined. It is almost certain that the measured initial track length is shorter than the "actual" initial length, and any such difference cannot be corrected for exactly by changing the parameters in Equation 10. We describe in Appendix B an attempt to find a better value for the initial track length by a method analogous to that used by Laslett and Galbraith (1996). However, as with their results, the predictions were quite inconsistent, with corrections to the measured initial lengths ranging from 5 to 15%. In any event, results discussed above imply that errors resulting from a slightly inaccurate initial track length value are probably minor.

Although Equation 8 successfully describes the relative amounts of annealing for two apatites at laboratory time scales, it remains to be seen whether it persists to geological time scales. Analysis of the laboratory data shows that there is probably a small time residual in some cases (Fig. 6). However, linear extrapolation of these residuals suggests that they may be very small, perhaps on the order of 0.03 for the difference in pre-

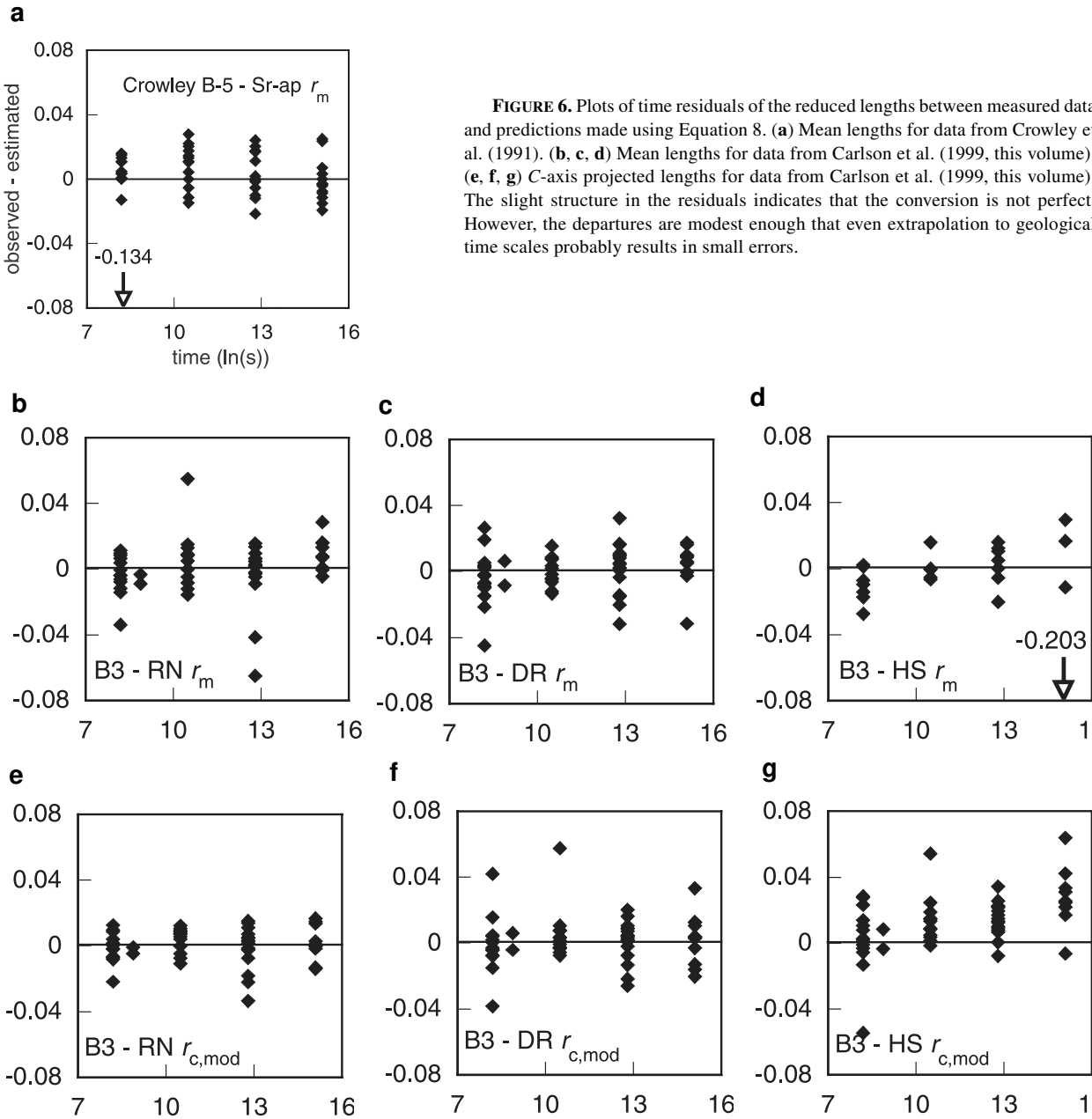

FIGURE 6. Plots of time residuals of the reduced lengths between measured data and predictions made using Equation 8. (**a**) Mean lengths for data from Crowley et al. (1991). (**b**, **c**, **d**) Mean lengths for data from Carlson et al. (1999, this volume). (**e**, **f**, **g**) *C*-axis projected lengths for data from Carlson et al. (1999, this volume). The slight structure in the residuals indicates that the conversion is not perfect. However, the departures are modest enough that even extrapolation to geological time scales probably results in small errors.

dicted reduced track length over time scales of 1–100 m.y. for apatites RN and DR. The most practical gauge of the effects of using Equation 8 is to compare the geological predictions of a model using the relation to simultaneously model all apatites to the predictions of models fitted to individual apatites. As shown below, this difference appears to be within the noise of the extrapolation.

If the apatite-apatite relationships observed in the laboratory were to hold over geological time scales for two apatites, it would imply that they shared exactly the same family of contours of constant length reduction on the Arrhenius plot, with the only difference being that the contour lines would represent different values for the two apatites. For example, in a parallel Arrhenius model, all contours for both apatites would have the same slope, whereas if a fanning Arrhenius model were correct, all contours for both apatites would fan from the same point. The effect of the transformations of length with the function g and the apatite-apatite fitting Equation 8 would be to ascribe values to these contours.

In their analysis, Laslett and Galbraith (1996) chose to effectively exclude this possibility by assuming explicitly that it is preferable that the length-transformation function be constant for all apatites. In doing so they imply that differences in annealing behavior among apatites should be explained primarily by differences in the function f of time and temperature, with perhaps some influence by the initial length, rather than

TABLE 5a. Geological time scale predictions from mean length fanning Arrhenius model based on mean lengths cell apatites studied

Apatite	$T_{F,100}$	$T_{F,30}$	$T_{F,10}$	$T_{C,1}$	$T_{C,10}$	$T_{C,100}$	$T_{A,1}$	$T_{A,10}$	$T_{A,100}$	T err	$l_{m,low\text{-}T}$	$l_{m,FC}$
HS	101.4	107.8	113.8	102.8	116.1	130.4	117.0	130.1	144.1	1.3–1.5	—	—
SC	103.8	110.2	116.3	108.7	122.3	136.8	119.5	132.7	146.7	1.3–1.5	15.19	—
RN	104.8	111.3	117.3	108.4	121.9	136.4	120.6	133.7	147.8	1.3–1.5	15.35	—
WK	110.5	117.0	123.1	112.6	126.2	140.9	126.3	139.6	153.8	1.4–1.6	15.07	—
OL	110.9	117.4	123.5	111.3	124.8	139.4	126.7	140.0	154.2	1.4–1.6	15.42	—
UN	111.8	118.3	124.5	112.0	125.5	140.1	127.7	141.0	155.2	1.4–1.6	15.23	—
PQ	114.2	120.8	126.9	113.3	126.9	141.5	130.1	143.5	157.8	1.4–1.6	14.81	—
DR	117.5	124.1	130.3	121.5	135.4	150.3	133.5	146.9	161.3	1.3–1.7	—	—
AY	120.1	126.7	132.9	121.9	135.8	150.7	136.1	149.6	164.0	1.3–1.8	—	—
FC	148.3	155.2	161.7	142.0	156.3	171.7	164.7	178.8	193.7	1.4–2.1	—	15.60
KP	158.0	165.0	171.5	149.5	164.0	179.5	174.6	188.8	203.9	1.5–2.2	—	—
B3	166.4	173.4	180.1	149.5	163.9	179.3	183.1	197.4	212.7	1.4–2.3	—	—
TI	189.8	197.0	203.9	164.7	179.4	195.1	206.8	221.5	237.2	1.5–2.3	—	—
PC	201.5	208.9	215.8	174.8	189.7	205.7	218.7	233.6	249.4	1.5–2.3	—	—
B2	207.9	215.3	222.2	180.3	195.3	211.4	225.1	240.1	256.0	1.5–2.2	—	—

TABLE 5b. Geological time scale predictions from mean length fanning Arrhenius model based on mean lengths cell apatites studied

Apatite	$T_{F,100}$	$T_{F,30}$	$T_{F,10}$	$T_{C,1}$	$T_{C,10}$	$T_{C,100}$	$T_{A,1}$	$T_{A,10}$	$T_{A,100}$	T err	$l_{m,low\text{-}T}$	$l_{m,FC}$
HS	66.9	75.7	83.8	71.5	88.5	106.8	86.0	103.5	121.8	1.7–2.1	—	—
SC	69.4	78.1	86.3	76.8	94.3	113.0	88.5	106.0	124.4	1.7–2.1	14.39	—
RN	70.4	79.2	87.4	76.6	94.0	112.6	89.6	107.1	125.5	1.7–2.1	14.51	—
WK	76.1	84.9	93.2	80.8	98.3	117.1	95.3	113.0	131.5	1.8–2.2	14.27	—
OL	76.5	85.3	93.6	79.6	97.0	115.7	95.7	113.4	132.0	1.7–2.2	14.55	—
UN	77.4	86.3	94.6	80.4	97.8	116.5	96.7	114.4	133.0	1.8–2.2	14.37	—
PQ	79.8	88.7	97.0	81.7	99.1	117.8	99.1	116.9	135.5	1.8–2.3	13.98	—
DR	83.1	92.1	100.4	89.2	107.2	126.4	102.5	120.4	139.1	1.8–2.3	—	—
AY	85.7	94.7	103.1	89.8	107.7	126.8	105.1	123.0	141.8	1.8–2.4	—	—
FC	113.7	123.0	131.7	109.6	128.1	147.8	133.6	152.1	171.5	1.9–3.1	—	14.96
KP	123.3	132.7	141.5	117.0	135.7	155.6	143.3	162.0	181.6	2.0–3.2	—	—
B3	131.6	141.1	149.9	117.3	135.8	155.5	151.7	170.6	190.3	2.0–3.3	—	—
TI	154.6	164.4	173.4	132.1	151.1	171.2	175.0	194.4	214.6	2.1–3.5	—	—
PC	166.1	176.0	185.2	141.9	161.2	181.6	186.7	206.2	226.7	2.2–3.5	—	—
B2	172.3	182.2	191.5	147.2	166.7	187.2	192.9	212.6	233.1	2.2–3.5	—	—

TABLE 5c. Geological time scale predictions from mean length fanning Arrhenius model based on mean lengths cell apatites studied

Apatite	$T_{F,100}$	$T_{F,30}$	$T_{F,10}$	$T_{C,1}$	$T_{C,10}$	$T_{C,100}$	$T_{A,1}$	$T_{A,10}$	$T_{A,100}$	T err	$l_{m,low\text{-}T}$	$l_{m,FC}$
HS	105.9	112.3	118.3	112.7	126.2	140.8	121.6	134.7	148.7	0.9–1.1	—	—
RN	114.2	120.6	126.7	123.6	137.5	152.4	130.0	143.2	157.3	0.9–1.1	15.38	—
SC	117.4	123.9	130.0	126.5	140.5	155.4	133.2	146.5	160.7	1.0–1.1	15.19	—
OL	118.6	125.2	131.3	127.0	140.9	155.9	134.5	147.8	162.0	1.0–1.1	15.49	—
WK	119.3	125.9	132.0	128.7	142.7	157.8	135.2	148.5	162.8	1.0–1.1	15.13	—
UN	119.8	126.3	132.5	128.2	142.2	157.2	135.7	149.0	163.3	1.0–1.1	15.31	—
PQ	123.3	129.8	136.0	131.5	145.5	160.6	139.2	152.6	166.9	1.0–1.1	14.92	—
DR	125.7	132.2	138.4	136.5	150.7	166.0	141.6	155.1	169.4	1.0–1.2	—	—
AY	126.8	133.4	139.6	136.7	150.9	166.2	142.8	156.3	170.6	1.0–1.2	—	—
FC	155.6	162.4	168.8	161.2	175.8	191.5	171.9	185.9	200.7	1.1–1.4	—	15.62
KP	159.1	166.0	172.5	165.4	180.1	195.9	175.5	189.5	204.4	1.1–1.4	—	—
B3	163.3	170.2	176.7	163.9	178.5	194.1	179.7	193.8	208.7	1.1–1.4	—	—
TI	233.3	240.6	247.5	216.9	232.2	248.5	250.4	265.3	281.0	1.3–1.5	—	—
PC	245.6	253.0	259.9	229.1	244.6	261.0	262.8	277.8	293.6	1.4–1.6	—	—
B2	255.4	262.8	269.8	236.2	251.8	268.3	272.6	287.7	303.6	1.4–1.9	—	—

TABLE 5d. Geological time scale predictions from mean length fanning Arrhenius model based on mean lengths cell apatites studied

Apatite	$T_{F,100}$	$T_{F,30}$	$T_{F,10}$	$T_{C,1}$	$T_{C,10}$	$T_{C,100}$	$T_{A,1}$	$T_{A,10}$	$T_{A,100}$	T err	$l_{m,low\text{-}T}$	$l_{m,FC}$
HS	72.3	81.0	89.2	81.4	98.9	117.5	91.4	108.8	127.0	1.2–1.4	—	—
RN	80.6	89.4	97.7	91.8	109.9	129.0	99.8	117.4	135.8	1.2–1.4	14.61	—
SC	83.9	92.7	101.0	94.7	112.8	132.1	103.1	120.7	139.2	1.3–1.5	14.43	—
OL	85.1	94.0	102.3	95.3	113.4	132.6	104.4	122.0	140.5	1.3–1.5	14.70	—
WK	85.8	94.7	103.0	96.9	115.1	134.4	105.1	122.7	141.2	1.3–1.5	14.42	—
UN	86.3	95.2	103.5	96.5	114.6	133.9	105.6	123.2	141.7	1.3–1.6	14.54	—
PQ	89.8	98.7	107.0	99.7	117.9	137.3	109.1	126.8	145.4	1.3–1.6	14.21	—
DR	92.2	101.1	109.4	104.5	123.0	142.6	111.5	129.3	147.9	1.3–1.6	—	—
AY	93.3	102.3	110.6	104.8	123.2	142.8	112.7	130.5	149.1	1.3–1.6	—	—
FC	122.0	131.2	139.8	129.1	148.0	168.1	141.7	160.0	179.1	1.4–2.0	—	15.05
KP	125.5	134.8	143.4	133.2	152.3	172.4	145.2	163.6	182.8	1.5–2.0	—	—
B3	129.6	138.9	147.5	131.9	150.8	170.8	149.4	167.8	187.1	1.5–2.1	—	—
TI	196.9	206.7	215.8	183.2	202.9	223.7	217.3	236.7	256.9	1.6–2.3	—	—
PC	208.3	218.2	227.4	194.7	214.6	235.6	228.8	248.3	268.6	1.6–2.3	—	—
B2	217.3	227.2	236.4	201.3	221.4	242.4	237.9	257.5	277.9	1.6–2.2	—	—

TABLE 5e. Parameters for models based on all apatites studied

Data	Model	χ^2_υ	C_0	C_1	C_2	C_3	α	β
l_m	F.A.	2.84	–11.053 (00744)	3.8964e-4 (02870)	–17.842 (02428)	6.7674e-4 (09207)	–0.14840	–8.7627
l_m	F.C.	2.92	–26.039 (04476)	0.53168 (09602)	–62.319 (12949)	–7.8935 (59139)	–0.20196	–7.4224
$l_{c,mod}$	F.A.	4.53	–9.0722 (04114)	2.9896e-4 (01537)	–15.846 (01656)	7.6370e-4 (05923)	–0.05771	–13.218
$l_{c,mod}$	F.C.	4.69	–19.844 (02202)	0.38951 (04539)	–51.253 (12954)	–7.6423 (58713)	–0.12327	–11.988

F.A. = Fanning Arrhenius model. F.C. = Fanning curvilinear model. Numbers in parentheses represent parameter variation within 95% confidence intervals.

the transform function *g*. The results presented here suggest that the transform function may play a more significant role than their approach allows, leading us to maintain flexibility in that part of the solution.

MULTIKINETIC MODELS

Table 5 shows the results of fitting all of the data presented in Carlson et al. (1999, this volume) with the same functions that were used earlier in this paper, utilizing Equation 8 and the simultaneously fit r_{mr0}-κ parameters from Table 4. Comparison of the results of the individual models for RN, DR, B3, and HS presented in Table 3 reveals that in most cases the match between the individually fit models and the corresponding simultaneous models is excellent. In the models based on mean track lengths, the maximum difference is <8 °C for apatites RN, DR, and B3. The congruence is better for these three apatites in the models based on *c*-axis projected lengths, in which the maximum difference is <5 °C for RN and B3 (and HS as well) and <7 °C for DR. The overall excellent correspondence leads us to conclude that although Equation 8 does not constitute a perfect extrapolation to geological time scales, it is easily good enough to provide an exceptional practical solution to the problem of characterizing multiple apatites.

As before, the fanning linear Arrhenius models fit the data from laboratory experiments slightly better than the curvilinear models. However, it also remains the case that the model that agrees best with the Otway Basin data is the fanning curvilinear model using *c*-axis projected lengths. Of the six near end-member F-apatites, half have $T_{F,30}$ temperatures that are in the 90–95 °C range, and the other three closely bracket that range. The new model also provides a reasonable match to the low-temperature benchmark based on Vrolijk et al. (1992), for which we now calculate values for each F-apatite with its own initial mean length, with the range being 14.21–14.70 μm. None of the models provide an exact match to the measured length of the Fish Canyon apatite (15.35 ± 0.06 μm). Because of these considerations, we advocate this model as the best one for calculating time-temperature paths using data from unknowns.

Another interesting feature of all of the models is that some apatites (notably B2) have index temperatures in excess of 200 °C. While it should be recognized that these highest-temperature predictions of the models are the least constrained because of the relative dearth of data for the most-resistant apatites, this result is in apparent general agreement with the observations of Kohn and Foster (1996) on apatites from the Stillwater Complex. These authors reported a continuum of apatite Cl contents from nil to the Cl-end-member, and found that apatites with mid-level Cl contents had the highest single-grain ages and were thus presumably the most resistant to annealing, as is the case with apatite B2 studied here. These intermediate-Cl apatites yielded fission-track ages that were concordant with zircon fission-track ages. Because of the slow cooling history undergone by the Stillwater Complex, these results suggest that such apatites may indeed have closure temperatures approaching those of zircon, which are constrained loosely to the range of 240 ± 50 °C (Hurford 1986), although work continues on this matter (Green et al. 1996; Johnson 1996; Foster et al. 1996).

Relating the model to kinetic indicators

Ideally, the final component of a multikinetic model would be a reliable conversion between measurable parameters, such as apatite composition or solubility, and the r_{mr0} and κ variables that describe relative annealing behavior. As shown above, r_{mr0} in particular is an excellent single parameter for characterizing relative resistance to annealing at laboratory time scales, and it seems to provide a reasonable estimate for geological time scales as well. However, this task is not straightforward.

Figure 7 shows the relationship between r_{mr0} (for *c*-axis projected lengths) and three possible kinetic indicators: Cl, D_{par} (diameter of etch figures parallel to the crystallographic *c*-axis) and OH. The chemical species are plotted so that the axis of symmetry for Cl suggested by the data of Kohn and Foster (1996), in which the maximum resistance to annealing was observed at mid-level rather then end-member composition, is folded back upon itself. The primary kinetic variable that has been described in the literature to date is Cl content, an increase in which supposedly leads to increased resistance to annealing (Green et al. 1986; Green 1995). Although our results corroborate this general trend, for the apatites studied here, Cl content is not by itself a robust predictor of kinetic behavior. This can be appreciated best by comparing the five apatites with low- to mid-level Cl content: AY, DR, FC, HS, and TI. At the low end, apatite HS has 0.10 apfu Cl as opposed to 0.12 for apatite DR, but has index temperatures that are some 15–25 °C lower, and is less resistant to annealing than even the end-member F-apatites. Apatite DR, on the other hand, has index temperatures some 5–15 °C higher than the F-apatites. Apatite AY has twice the Cl content of DR, but is virtually identical in terms of its resistance to annealing. Apatite FC has roughly equivalent Cl to AY, but is much more resistant to annealing, with predicted index temperatures some 20–30 °C higher. Finally, apatite TI has less Cl than AY and FC, but a much higher resistance to annealing than either one.

Some of these inconsistencies clearly are caused by the influence of other chemical factors. For example, the fact that apatite HS is a near-end-member hydroxyapatite could reasonably be inferred to override the influence of its Cl content. The compositional differences responsible for the relative behavior of the other apatites are more subtle, however. It is clear that

cation substitutions also can play a large role in determining kinetic behavior; the Mn-fluorapatite PC has no Cl but is among the most resistant to annealing that we studied. Although high levels of most cation substitutions are rare, most of the differences that may cause the varying behavior of the chlorapatites we studied are minor, and the levels are within the range of common observations (Carlson et al. 1999, this volume).

Examination of the data presented here reveals that resistance to annealing cannot be reproduced by a simple linear combination of individual compositional variables. The fact that apatites B2, PC, and TI have similar annealing behaviors despite their very different compositions suggests that they may be close to the limit of apatite resistance to annealing for any composition. It is likely that there is a point where addition of Cl or various cations becomes less effective in increasing resistance to annealing, or even starts to shift the kinetics in the opposite direction. For this reason, plus the fact that many potentially important

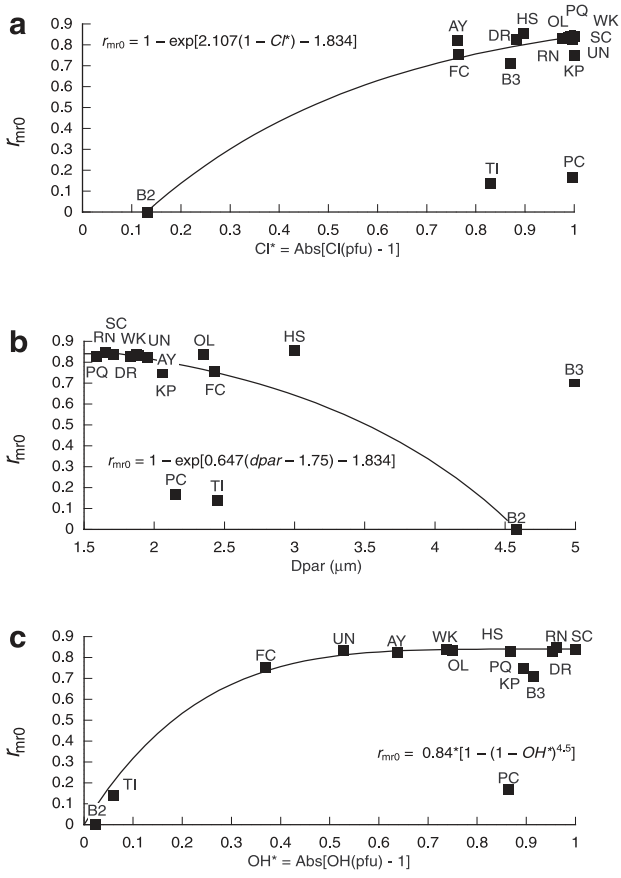

FIGURE 7. Suggested relations between r_{mr0} and possible indicators of kinetic behavior: (**a**) Cl; (**b**) D_{par} (etch figure length parallel to the crystallographic *c* axis); and (**c**) OH. Cl and OH are plotted in terms of formula units, and assume an axis of symmetry around the mid-level composition of each one, as suggested by the results of Kohn and Foster (1995) for Cl-apatites in the Stillwater complex. The only apatites affected by the plotting method are B3 in part **a** and HS in part **c**. The Cl and D_{par} curves produce an approximately linear relationship between kinetic parameters and index temperatures between end-member fluorapatite and B2 Cl-OH apatite. The OH curve is fit to the data and does the best job of fitting all but the most unusual apatites in this study. However, it is uncertain if OH is in fact the best overall kinetic indicator.

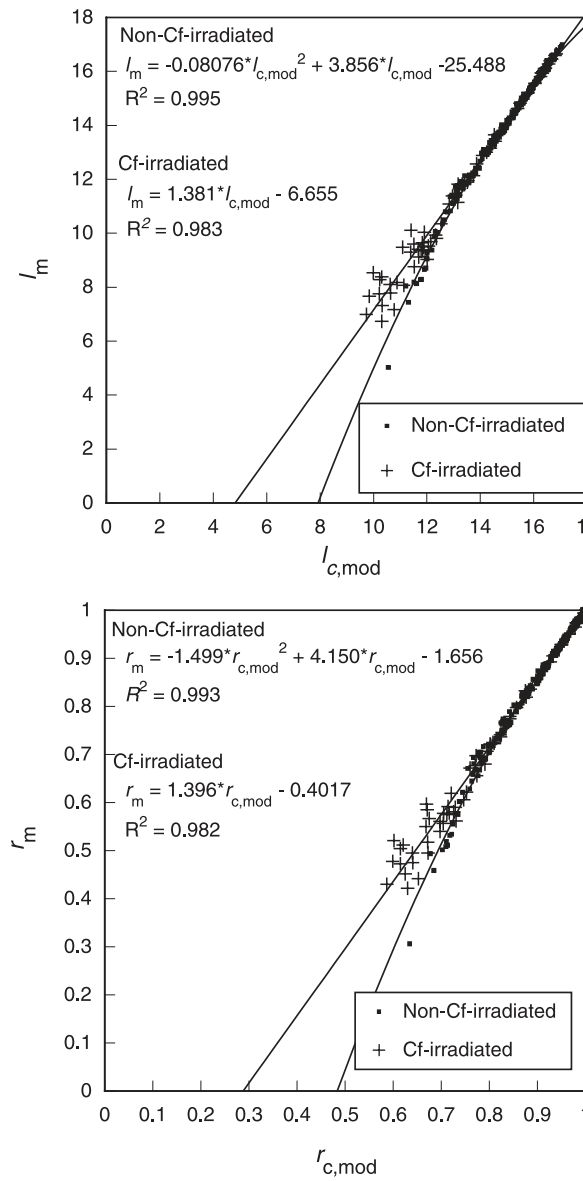

FIGURE 8. Relation between mean and modeled *c*-axis projected lengths (**a**) and reduced lengths (**b**) for the apatites in this study. These curves can be used to create a mean-length model that corresponds to a *c*-axis projected model, and to predict the amount of mean-length biasing in studies where modeled *c*-axis projected lengths are used. Different curves are fit to experiments that have and have not been Cf-irradiated; Cf-irradiation is an effective tool for obtaining data from highly annealed samples, but can alter length-biasing effects in a non-systematic way, leading to the observed scatter. Most of the biasing effect can be removed by using modeled *c*-axis projected lengths.

compositional variables are described by only one or two apatites, the multivariate equation for r_{mr0} provided by Carlson et al. (1999, this volume) is not advisable for general use in estimating the annealing behavior of unknown apatites.

Although the currently available parameters for inferring kinetic behavior are demonstrably imprecise with respect to the apatites examined in this study, practical experience tells us that they are nonetheless useful, and can provide important constraints for modeling time-temperature paths in many natural situations. Thus we present in Figure 7 a series of suggested empirical relations between the resistance-to-annealing parameter r_{mr0} and the possible kinetic indicators. In all three cases, once r_{mr0} is known, Equation 9 is used to determine κ. For the Cl model, we define a curve between end-member F-apatite and B2 (Cl-OH) apatite, which is the most resistant to annealing. Because of the scatter of behavior in the low-Cl apatites, and our lack of apatites with Cl contents between 0.24 and 0.87 apfu, we take as our main indicator of the change in annealing behavior with respect to increasing Cl content the fact that the Stillwater Complex apatites studied by Kohn and Foster (1996) showed smoothly and roughly linearly increasing ages from end-member F-apatite to mid-level Cl-apatite. The function given in Figure 7a produces a roughly linear trend between fading temperature and increasing Cl content. We use the same approach for the model based on D_{par} (Fig. 7b), and the function defined approximates a roughly linear trend between etch pit diameter and fading temperature. For each of these two relations, it should be recognized that the uncertainty in inferred closure temperature increases markedly as the values of the kinetic indicators increase. Neither of the relations are robust, and each fails for different types of apatite. Both fail for apatites with unusually large amounts of cation substitutions (PC and KP), and for near-end-member chlorapatite (B3); however, all of these varieties are very rare (Carlson et al. 1999, this volume). The D_{par} relation is prone to error if there is a large hydroxyl component, which evidently can lead to enhanced solubility without a corresponding increase in annealing resistance, such as for apatites HS and OL. On the other hand, D_{par} is apparently more reliable in the sense that all apatites studied with etch figures <2 μm in diameter have a low resistance to annealing, whereas apatites with low Cl content have the potential to encompass the full range of possible kinetic behaviors.

Figure 7c shows that using OH content as the kinetic variable yields an intriguing relation that apparently fits all but three of the apatites we studied (PC, KP, and B3). However, we have no independent evidence that points to hydroxyl as the governing kinetic parameter, and some evidence that suggests the contrary. It should also be pointed out that the OH-based model really matches only the relative lack of variation among nine of the apatites we studied and the trend defined by three of the remaining six. There is a broad correlation in many cases between increased contents of Cl and OH. This relation can lead to apparent trends of resistance to annealing that increase with one variable but are in fact caused by the kinetic effects of the other. The OH component is the most difficult to quantify in apatite using microprobe analysis, because it must be obtained by difference through stoichiometric calculations after all other chemical species have been measured, which can be problematic (e.g., Stormer et al. 1993).

Modeling projected vs. mean lengths

There are several complexities that must be recognized and addressed carefully if a *c*-axis projected-length model is to be used to derive time-temperature information from natural specimens. If track orientations are measured, investigators must ensure that the *c* axis of the apatite being measured is in the plane of the polished section, and some calibration may be required to account for the effects that different etching and measurement procedures could have on the observed track-length anisotropy. Calculating estimated time-temperature paths would also require a scheme that accounts for the relative probability of observing different track populations in unknowns. A computer model typically divides a time-temperature path into a set of discrete segments and traces the annealing history of the track length population formed during each segment (Willett 1992, 1997; Crowley 1993a). Because early formed track populations will be shortened relative to later-formed populations, they are less likely to be observed and measured. This biasing usually is approximated as being directly proportional to the mean track length, although a more detailed model that includes the effects of track orientation may provide a more correct answer.

There are two possible approaches to these issues. One is to use a conversion from projected lengths to mean lengths to estimate biasing effects, and another is to use this same conversion to transform the projected-length model into a mean-length one. Two conversions based on the data presented in Carlson et al. (1999, this volume) are shown in Figure 8. For the analyses that were not Cf-irradiated, the data follow a very tight trend that is well described by a second-degree polynomial. For Cf-irradiated experiments that show evidence of segmentation, the data follow a more linear trend but become more diffuse with increasing annealing, presumably owing to biasing effects of the procedure that alter the relative probability of measuring fission tracks with different sizes and orientations. Until this bias is better understood and quantified, for Cf-irradiated analyses the linear function should be used and an error term introduced into the modeling program to account for the uncertainty.

Etching methods

The particular etching method used for generating the data that form the basis of this model (Carlson et al. 1999, this volume) is currently not in wide use in the fission-track community, and it is likely that most investigators will not want to change their methodology. Investigators seeking to use this model to interpret fission-track data should keep in mind possible ways that different etching techniques can affect data. The routine calibration of measuring spontaneous and induced fission-track lengths in standard apatites and using these values to normalize model predictions will likely suffice for correction of calculations involving mean lengths. However, insofar as etching technique influences the anisotropy of etch figures, it may also have an effect on *c*-axis projection (e.g., Donelick et al. 1999, this volume). If investigators employing alternate etching techniques wish to use *c*-axis projected lengths for modeling, additional calibrations may be necessary.

DISCUSSION

The multikinetic annealing model developed in this paper is primarily a practical construct, geared to aid in the interpre-

tation of fission-track data by maximizing consistency with both laboratory data and geological benchmarks. A well-conceived empirical model can also be used to gain insight into the underlying physical processes. Other investigators have tried to derive physical meaning from aspects of their empirical models, such as interpreting the fanning point in a fanning Arrhenius model as the physical limit of fission-track stability (Crowley et al. 1991; Crowley 1993b), or making the initial track length a fitted parameter (Laslett and Galbraith 1996). These specific usages may be overly optimistic. For example, the use of a single fanning point from which all contours of equal annealing originate was proposed as a mathematical simplification, not a physical postulate (Laslett et al. 1987). The use of a fanning Arrhenius model to estimate the initial fission-track length relies on the assumption that the empirical approximation is correct enough both in principle and in particulars to extract a fairly subtle physical detail.

However, the results of the empirical approach may help guide the way to understanding the underlying physical process in a broader sense. The results of this study are of interest in that they corroborate the finding that contours of constant annealing fan on an Arrhenius plot, suggest that these contours have a certain amount of curvature, and suggest that seemingly subtle chemical variations can have a large effect on the slope of these contours at high levels of annealing. We offer here the outline of a possible explanation for these observations in the context of a defect-elimination model (i.e., Gold et al. 1981; Carlson 1990), although we recognize that other physical explanations such as surface-energy minimization may apply (e.g., Donelick et al. 1999, this volume). The central component of our idea is that fission tracks are composed of a wide range of possible defects, each of which may have a different activation energy for annealing. The activation energy for annealing of a single defect is a function of the energy level of a displaced atom in its interstitial site and the energy barrier that the surrounding crystal structure presents to the return of that atom to a normal site. Given that there may be a wide range of impurities and a near-infinitude of possible arrangements of interstitial sites and semi-intact structure, it is easy to envision that a fairly continuous and smooth distribution of activation energies may exist that are required to cause annealing of fission tracks. [Similar conjectures are made by Green et al. (1988), although those authors argued against trying to characterize fission-track annealing with models having a theoretical physical basis in favor of simpler empirical approaches.] Furthermore, insofar as a high activation energy implies a large amount of energy deposition from the fission particle to the crystal structure, it is possible that the mean and maximum activation energies of the defects comprising a fission track may fall off toward its ends.

Such a model may explain the fanning of annealing contours by postulating that a fission track may anneal by progressive elimination of the lower-energy defects initially and higher-energy defects at later stages. The fact that early annealing proceeds via tip shortening may reflect a smaller diameter for the outer parts of the track (e.g., Carlson 1990) or lower-energy defects there as hypothesized above, or some combination of the two. Because it is probable that annealing with respect to etching requires simply falling below some threshold defect density rather than elimination of all defects, the persistence of some high-energy defects need not present a problem.

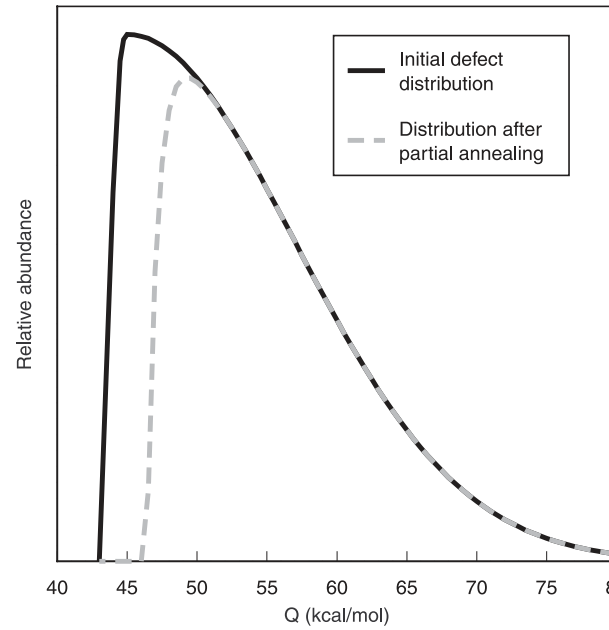

FIGURE 9. Schematic illustration of the possible kinetic implications of a fission track being composed of defects that have a range of activation energies for annealing. The solid curve is a hypothetical initial distribution of activation energies for defect elimination, and the dashed curve is the distribution after an arbitrary isothermal annealing episode calculated using Equation 12. The resulting distribution has three parts: on the left side, all of the low-activation-energy defects have been annealed; in a narrow middle portion, the annealing rates are similar; and on the right side, annealing rates are comparatively negligible for the temperature and time scale modeled.

The kinetic effects of compositional variations can shift the distribution of activation energies. For example, the small ionic radius cations Fe^{2+} (or Fe^{3+}) and Mn^{2+} (or Mn^{3+}) may be more stable in interstitial sites than Ca^{2+}, and thus require a higher activation energy to be displaced. Ordering requirements for mixtures in the anion site (e.g., Hughes et al. 1989) may present a different kind of energy barrier to annealing.

Finally, the curvature that we infer to exist based on comparing the laboratory data to geological examples may have had some foreshadowing in the model of Carlson (1990). The primary constitutive equation of the model (Carlson 1990, Eq. 2) is:

$$\frac{\mathrm{d}N}{\mathrm{d}t} = -c\left(\frac{\mathrm{k}T(t)}{\mathrm{h}}\right)\exp\left(\frac{-Q}{\mathrm{R}T(t)}\right) \qquad (11)$$

where $\mathrm{d}N/\mathrm{d}t$ is the defect elimination rate, c is an empirical rate constant, k is Boltzmann's constant, h is Planck's constant, T is absolute temperature, t is time since the beginning of the annealing episode, R is the universal gas constant, and Q corresponds to an activation energy. The temperature term in the pre-exponential constant, which helps define the rate at which

the activation energy barrier is assailed, causes the contours of constant annealing on an Arrhenius diagram to curve in the final form of the Carlson (1990) model, as opposed to the linear contours that would arise from the exponential term alone. In that model, the pre-exponential temperature term is insignificant compared to the exponential term, and the degree of curvature in terms of change in contour slope from laboratory to geological time scales is ~2–3%, as opposed to the ~35–40% present in the fanning curvilinear model. If we approximate a range of activation energies by replacing the single value with a summation, the equation becomes:

$$\frac{dN}{dt} = -c\left(\frac{kT(t)}{h}\right)\sum_i w_i(t)\exp\left(\frac{-Q_i}{RT(t)}\right) \qquad (12)$$

where w_i is a weighting factor reflecting the proportion of defects at activation energy Q_i as time progresses. An example of the influence of the variation on activation energies in Equation 12 is shown in Figure 9. Because of the exponential dependence of the defect-elimination rate on the activation energy, at any temperature only defects within a relatively narrow range of activation energies (perhaps 3–4 kcal/mol) will anneal at similar rates at any one time; lower-energy defects will have annealed already, and higher-energy defects will anneal at a comparatively negligible rate. On laboratory time scales, activation energies inferred from Arrhenius-type plots vary by 10–35 kcal/mol for any single type of apatite. The smaller proportion of defects that are actively annealing at any given time causes the pre-exponential temperature term to rise in significance compared to the exponential one, which in turn would make the equation more similar to an empirical fanning curvilinear model and lead to greater curvature of contours on an Arrhenius diagram. This approach has a precursor in the work of Bertel and Mark (1983), who used multiple exponential decay functions to model fission-track density reduction.

To create a model following this approach, it would be necessary to quantify the distribution of activation energies in a single fission track, the distribution of defects and energies along the length of a track and perhaps radially as well, the concentration of defects required to accelerate etching, and the activation-energy effects of the various possible cation and anion substitutions. A similar strategy is used to model vitrinite maturation and reflectance (Sweeney and Burnham 1990; Burnham and Sweeney 1989), in which different chemical reactions are each assigned a range of activation energies.

Of equal importance to an improved physical model of fission-track annealing is a more robust database of geological benchmarks. Indeed, we feel that the most significant weakness of the work presented here is that, although it is based on the largest set of annealing experiments published to date, it relies on too few relevant geological data. For example, as discussed previously, the fission-track down-hole fading temperatures in southern Texas reported by Corrigan (1993) appear likely to be incompatible with those from the Otway Basin. It should be noted that, because fission-track lengths tend to be most influenced by the highest temperatures they have experienced, unaccounted-for heating events can have a large effect on the results of down-hole fading studies. This inherent error bias will tend to make higher-temperature estimates more credible, as over geological time it is difficult to have absolute confidence that some transitory heating event has not occurred. With the sparsity of geological data now publicly available it is impossible to make any definitive judgments, but these issues highlight the importance of developing a varied database to constrain confidently the behavior of fission tracks at geological time scales with the accuracy desired for economic applications.

We note in closing that if the physical model discussed above is sound, it would predict that contours of constant annealing become more linear at higher levels of annealing, as a progressively higher proportion of the remaining defects will be annealing actively. Such a model would show similar low-temperature behavior to our empirical fanning-curvilinear model while raising the predicted index temperatures.

ACKNOWLEDGMENTS

This research was supported by Grant 28367-AC2 from the American Chemical Society—Petroleum Research Fund to WDC, and by Donelick Analytical, Inc. The Geology Foundation of the University of Texas at Austin helped to defray costs of publication. We thank Sean Willett for some of the computational techniques used. Insightful reviews by Mark Brandon, Jeff Corrigan, Paul O'Sullivan, and Robert Dymek improved the manuscript.

REFERENCES CITED

Bertel, E. and Mark, T.D. (1983) Fission tracks in minerals: Annealing kinetics, track structure and age correction. Physics and Chemistry of Minerals, 9, 197–204.

Box, G.E.P. and Cox, D.R. (1964) An analysis of transformations. Journal of the Royal Statistical Society B, 26, 211–252.

Burnham, A.K. and Sweeney, J.J. (1989) A chemical model of vitrinite maturation and reflectance. Geochimica at Cosmochimica Acta, 53, 2649–2657.

Burtner, R.L., Nigrini, A., and Donelick, R.A. (1994) Thermochronology of lower Cretaceous source rocks in the Idaho-Wyoming Thrust Belt. American Association of Petroleum Geologists Bulletin, 78, 1613–1636.

Carlson, W.D. (1990) Mechanisms and kinetics of apatite fission-track annealing. American Mineralogist, 75, 1120–1139.

———(1993) Mechanisms and kinetics of apatite fission-track annealing—Reply to Kevin D. Crowley. American Mineralogist, 78, 213–215.

Carlson, W.D., Donelick, R.A., and Ketcham, R.A. (1999) Variability of apatite fission-track annealing kinetics: I. Experimental results. American Mineralogist, 84, 1213–1223.

Corrigan, J.D. (1990) On apatite fission-track analysis and heat transfer processes in the upper crust, 241 p. Ph.D. dissertation, University of Texas, Austin.

———(1991) Inversion of apatite fission track data for thermal history information. Journal of Geophysical Research, 96, 10347–10360.

———(1993) Apatite fission-track analysis of Oligocene strata in South Texas, U.S.A.: Testing annealing models. Chemical Geology, Isotope Geoscience Section, 104, 227–249.

Crowley, K.D. (1993a) Lenmodel: a forward model for calculating length distributions and fission-track ages in apatite. Computers and Geosciences, 19, 619–626.

———(1993b) Mechanisms and kinetics of apatite fission-track annealing—Discussion. American Mineralogist, 78, 210–212.

Crowley, K.D., Cameron, M., and Schaefer, R.L. (1991) Experimental studies of annealing etched fission tracks in fluorapatite. Geochimica et Cosmochimica Acta, 55, 1449–1465.

Dodson, M.H. (1973) Closure temperature in cool geochronological and petrological systems. Contributions to Mineralogy and Petrology, 40, 259–274.

———(1979) Theory of cooling ages. In E. Jager and J.C. Hunziker, Eds., Lectures in Isotope Geology, p. 194–202. Springer, New York.

Donelick, R.A. (1991) Crystallographic orientation dependence of mean etchable fission track length in apatite: An empirical model and experimental observations. American Mineralogist, 76, 83–91.

———(1993) A method of fission track analysis utilizing bulk chemical etching of apatite. U.S. Patent Number 6,267,274.

———(1995) A method of fission track analysis utilizing bulk chemical etching of apatite. Australian Patent Number 658,800.

Donelick, R.A. and Miller, D.S. (1991) Enhanced TINT fission track densities in low spontaneous track density apatites using ^{252}Cf-derived fission fragment tracks: A model and experimental observations. Nuclear Tracks and Radiation Measurements, 18, 301–307.

Donelick, R.A., Roden, M.K., Mooers, J.D., Carpenter, B.S., and Miller, D.S. (1990) Etchable length reduction of induced fission tracks in apatite at room temperature (~23°C): Crystallographic orientation effects and "initial" mean lengths. Nuclear Tracks and Radiation Measurements, 17, 261–265.

Donelick, R.A., Ketcham, R.A., and Carlson, W.D. (1999) Variability of apatite fission-track annealing kinetics II: Crystallographic orientation effects. American Mineralogist, 84, 1224-1234.

Foster, D.A., Kohn, B.P., and Gleadow, A.J.W. (1996) Sphene and zircon fission track closure temperatures revisited: empirical calibrations from $^{40}Ar/^{39}Ar$ diffusion studies of K-feldspar and biotite. International Workshop on Fission-Track Dating, Ghent, Abstracts, 37.

Gallagher, K. (1995) Evolving temperature histories from apatite fission-track data. Earth and Planetary Science Letters, 136, 421–435.

Gleadow, A.J.W. and Duddy, I.R. (1981) A natural long-term track annealing experiment for apatite. Nuclear Tracks and Radiation Measurements, 5, 169–174.

Gold, R., Roberts, J.H., and Ruddy, F.H. (1981) Annealing phenomena in solid state track recorders. Nuclear Tracks and Radiation Measurements, 5, 253–264.

Green, P.F. (1981) A new look at statistics in fission-track dating. Nuclear Tracks and Radiation Measurements, 5, 77–86.

———(1988) The relationship between track shortening and fission track age reduction in apatite: Combined influences of inherent instability, annealing anisotropy, length bias and system calibration. Earth and Planetary Science Letters, 89, 335–352.

———(1995) AFTA Today. OnTrack, 5 (November), 8–10.

Green, P.F., Duddy, I.R., Gleadow, A.J.W., Tingate, P.R., and Laslett, G.M. (1985) Fission-track annealing in apatite: track length measurements and the form of the Arrhenius plot. Nuclear Tracks and Radiation Measurements, 10, 323–328.

———(1986) Thermal annealing of fission tracks in apatite 1. A qualitative description. Chemical Geology, Isotope Geoscience Section, 59, 237–253.

Green, P.F., Duddy, I.R., and Laslett, G.M. (1988) Can fission track annealing in apatite be described by first-order kinetics? Earth and Planetary Science Letters, 87, 216–228.

Green, P.F., Duddy, I.R., Gleadow, A.J.W., and Lovering, J.F. (1989a) Apatite fission-track analysis as a paleotemperature indicator for hydrocarbon exploration. In N.D. Naeser and T.H. McCulloh, Eds., Thermal Histories of Sedimentary Basins: Methods and Case Histories, p. 181–195. Springer, New York.

Green, P.F., Duddy, I.R., Laslett, G.M., Hegarty, K.A., Gleadow, A.J.W., and Lovering, J.F. (1989b) Thermal annealing of fission tracks in apatite 4. Quantitative modeling techniques and extension to geological time scales. Chemical Geology (Isotope Geoscience Section), 79, 155–182.

Green, P.F., Hegarty, K.A., Duddy, I.R., Foland, S.S., and Gorbachev, V. (1996) Geological constraints on fission track annealing in zircon. International Workshop on Fission-Track Dating, Ghent, Abstracts, 44.

Harrison, T.M. (1985) A reassessment of fission-track annealing behavior in apatite. Nuclear Tracks and Radiation Measurements, 10, 329–333.

Hughes, J.M., Cameron, M., and Crowley, K.D. (1989) Structural variations in natural F, OH, and Cl apatites. American Mineralogist, 74, 870–876.

Hurford, A.J. (1986) Cooling and uplift patterns in the Lepontine Alps, south central Switzerland, and an age of vertical movement on the Insubric fault line. Contributions to Mineralogy and Petrology, 92, 413–427.

Issler, D.R. (1996) Optimizing time step size for apatite fission track annealing models. Computers and Geosciences, 22, 67–74.

Johnson, C. (1996) Zircon fission track annealing and quantitative thermal history modelling. International Workshop on Fission-Track Dating, Ghent, Abstracts, 60.

Kohn, B.L. and Foster, D.A. (1996) Exceptional chlorine variation in the Stillwater Complex, Montana: Thermochronological consequences. International Workshop on Fission-Track Dating, Ghent, Abstracts, 37.

Laslett, G.M. and Galbraith, R.F. (1996) Statistical modelling of thermal annealing of fission tracks in apatite. Geochimica et Cosmochimica Acta, 60, 5117–5131.

Laslett, G.M., Green, P.F., Duddy, I.R., and Gleadow, A.J.W. (1987) Thermal annealing of fission tracks in apatite 2. A quantitative analysis. Chemical Geology, Isotope Geoscience Section, 65, 1–13.

Naeser, C.W. (1981) The fading of fission tracks in the geologic environment—data from deep drill holes. Nuclear Tracks and Radiation Measurements, 5, 248–250.

Naeser, C.W. and Fleischer, R.L. (1975) Age of the apatite at Cerro de Mercado, Mexico: A problem for fission-track annealing corrections. Geophysical Research Letters, 2, 67–70.

Naeser, C.W. and Forbes, R.L. (1976) Variation of fission track ages with depth in two deep drill holes. EOS, 57, 363.

Naeser, C.W., Zimmerman, R.A., and Cebula, G.T. (1981) Fission-track dating of apatite and zircon: An interlaboratory comparison. Nuclear Tracks and Radiation Measurements, 5, 56–72.

O'Sullivan, P.B. and Parrish, R.R. (1995) The importance of apatite composition and single-grain ages when interpreting fission track data from plutonic rocks: a case study from the Coast Ranges, British Columbia. Earth and Planetary Science Letters, 132, 213–224.

Stormer, J.C. Jr., Pierson, M.L., and Tacker, R.C. (1993) Variation of F and Cl X-ray intensity due to anisotropic diffusion in apatite during electron microprobe analysis. American Mineralogist, 78, 641–648.

Sweeney, J.J. and Burnham, A.K. (1990) Evaluation of a simple model of vitrinite reflectance based on chemical kinetics. American Association of Petroleum Geologists Bulletin, 74, 1559–1570.

Vrolijk, P., Donelick, R.A., Queng, J., and Cloos, M. (1992) Testing models of fission track annealing in apatite in a simple thermal setting: site 800, leg 129. In R.L. Larson and Y. Lancelot, Eds., Proceedings of the Ocean Drilling Program, Scientific Results, 129, 169–176. Ocean Drilling Program, Texas A&M University, College Station, Texas.

Willett, S.D. (1992) Modelling thermal annealing of fission tracks in apatite. In M. Zentilli and P.H. Reynolds, Eds., Short Course Handbook on Low Temperature Thermochronology, p. 43–72. Mineralogical Association of Canada, Napean, Ontario.

———(1997) Inverse modeling of annealing of fission tracks in apatite 1: A controlled random search method. American Journal of Science, 297, 939–969.

MANUSCRIPT RECEIVED JUNE 8, 1998
MANUSCRIPT ACCEPTED MAY 4, 1999
PAPER HANDLED BY ROBERT F. DYMEK